Ca^{2+}-Mobility in the Sarcoplasmic Reticulum of Ventricular Myocytes Is Low

Pawel Swietach,* Kenneth W. Spitzer,† and Richard D. Vaughan-Jones*
*Burdon Sanderson Cardiac Science Centre, Department of Physiology, Anatomy, and Genetics, Oxford University, Oxford OX1 3PT, United Kingdom; and †Nora Eccles Harrison Cardiovascular Research and Training Institute, University of Utah, Salt Lake City, Utah 84112-5000

ABSTRACT The sarcoplasmic reticulum (SR) in ventricular myocytes contains releasable Ca^{2+} for activating cellular contraction. Recent measurements of intra-SR (luminal) Ca^{2+} suggest a high diffusive Ca^{2+}-mobility constant (D_{CaSR}). This could help spatially to unify SR Ca^{2+}-content ($[Ca^{2+}]_{SRT}$) and standardize Ca^{2+}-release throughout the cell. But measurements of localized depletions of luminal Ca^{2+} (Ca^{2+}-blinks), associated with local Ca^{2+}-release (Ca^{2+}-sparks), suggest D_{CaSR} may actually be low. Here we describe a novel method for measuring D_{CaSR}. Using a cytoplasmic Ca^{2+}-fluorophore, we estimate regional $[Ca^{2+}]_{SRT}$ from localized, caffeine-induced SR Ca^{2+}-release. Caffeine microperfusion of one end of a guinea pig or rat myocyte diffusively empties the whole SR at a rate indicating D_{CaSR} is 8–9 $\mu m^2/s$, up to tenfold lower than previous estimates. Ignoring background SR Ca^{2+}-leakage in our measurement protocol produces an artifactually high D_{CaSR} (>40 $\mu m^2/s$), which may also explain the previous high values. Diffusion-reaction modeling suggests that a low D_{CaSR} would be sufficient to support local SR Ca^{2+}-signaling within sarcomeres during excitation-contraction coupling. Low D_{CaSR} also implies that $[Ca^{2+}]_{SRT}$ may readily become spatially nonuniform, particularly under pathological conditions of spatially nonuniform Ca^{2+}-release. Local control of luminal Ca^{2+}, imposed by low D_{CaSR}, may complement the well-established local control of SR Ca^{2+}-release by Ca^{2+}-channel/ryanodine receptor couplons.

INTRODUCTION

The sarcoplasmic reticulum (SR) is the primary store of releasable Ca^{2+} within a mammalian myocyte. In ventricular cells, the SR is a reticular, luminally continuous compartment, occupying 3%–4% of cell volume (1,2). Free Ca^{2+}-ion concentration in the loaded SR ($[Ca^{2+}]_{SR}$) is probably 0.5–1.0 mM, 5000–10,000-fold higher (3) than diastolic Ca^{2+}-ion concentration in the cytoplasm ($[Ca^{2+}]_i$). Ca^{2+}-release from the SR is central to excitation-contraction coupling in the heart. It accounts for most of the cytosolic Ca^{2+}-transient required to activate the myofilaments (4). Release is controlled locally through couplons, small units composed of a sarcolemmal L-type Ca^{2+}-channel (LCC), closely apposed to several ryanodine receptor (RyR) channels in the SR membrane (5). Influx of extracellular Ca^{2+} through the LCC opens the attendant RyRs via a process of Ca^{2+}-induced Ca^{2+}-release, allowing a local release of Ca^{2+}, from SR to cytosol (4,5). Using fluorescent techniques, this release can be measured as a Ca^{2+}-spark (6). The synchronized operation of many thousands of couplons within a cardiac cell underpins the global Ca^{2+}-transient that is triggered by an action potential (4).

The local nature of SR Ca^{2+}-release via couplons is reinforced by a low cytoplasmic Ca^{2+}-mobility (~14 $\mu m^2/s$) (7), which limits the spatial spread of Ca^{2+} from its source. This ensures that rogue Ca^{2+}-sparks, when they occur randomly, do not readily induce a global Ca^{2+}-release from the SR. Although Ca^{2+} released at couplons is localized by low Ca^{2+}-mobility in cytoplasm, it is far from clear whether Ca^{2+}-movements are equally localized in the lumen of the SR. The use of a low-affinity Ca^{2+}-fluorophore, Fluo-5N, to measure ionized Ca^{2+}-concentration ($[Ca^{2+}]_{SR}$) within isolated cardiomyocytes, was pioneered by Bers and colleagues (8,9). Using this technique in rabbit ventricular myocytes, they and others have observed a transient fall of global $[Ca^{2+}]_{SR}$ (termed a Ca^{2+}-scrap (8)), which coincides with the electrically evoked cytosolic Ca^{2+}-transient.

Within a sarcomere, the time course of the scrap appears uniform throughout the SR, suggesting that high luminal Ca^{2+}-mobility may be minimizing local $[Ca^{2+}]_{SR}$ gradients. The result is of great interest, given that Ca^{2+} released from terminal cisternae of the junctional SR (jSR) is resequestered remotely by SR Ca^{2+}-ATPase (SERCA) pumps located on network SR (nSR) (2,10), which then diffusively feeds the Ca^{2+} back into the jSR, a recycling distance of 1–2 μm. The proposal for high SR Ca^{2+}-mobility (D_{CaSR}) has gained further support from Fluo-5N measurements of global Ca^{2+}-diffusion within the SR, suggesting D_{CaSR} is four- to fivefold higher (60 $\mu m^2/s$) (9) than Ca^{2+}-mobility in cytoplasm. Such high mobility would be occurring in the face of high SR tortuosity and high-capacity luminal buffers like calsequestrin, which are expressed in the jSR (2,11). A high D_{CaSR} has also been proposed recently to be necessary for the propagation of cytosolic Ca^{2+}-waves in cardiac cells subjected to intracellular Ca^{2+}-overload (12).

The concept of high D_{CaSR} appears to be challenged by the observation of local jSR Ca^{2+}-depletions (termed Ca^{2+}-blinks

Submitted January 28, 2008, and accepted for publication March 21, 2008.

Address reprint requests to Professor Richard D. Vaughan-Jones, PhD, Burdon Sanderson Cardiac Science Centre, Department of Physiology, Anatomy, and Genetics, Oxford University, Oxford OX1 3PT, UK. E-mail: richard.vaughan-jones@dpag.ox.ac.uk.

Editor: David A. Eisner.

0006-3495/08/08/1412/16 $2.00

doi: 10.1529/biophysj.108.130385

(2,13,14)), which coincide with the generation of cytosolic Ca^{2+}-sparks. A Ca^{2+}-blink is the luminal consequence of local jSR Ca^{2+}-release. The Ca^{2+}-blink occurs with no apparent change in adjacent nSR $[Ca^{2+}]_i$ (2) and recovers to control levels in 100–200 ms. If, as proposed (2,14), recovery is due to Ca^{2+}-diffusion from nSR to jSR, this implies significant resistance to luminal Ca^{2+}-movement, at least at the nSR-jSR junction. Such an arrangement would predict that global movement of Ca^{2+} throughout the SR, such as measured previously using Fluo-5N, would be rate limited by low mobility and high Ca^{2+}-buffering in the jSR. If this were so, the global D_{CaSR} would appear low, not high. A low global D_{CaSR} may also be compounded by the tenuous nSR that links successive sarcomeres within a myocyte (2) and that may functionally isolate adjacent SR pools of Ca^{2+}. In an attempt to resolve the apparently discrepant predictions for D_{CaSR}, we reexamined the question of global SR Ca^{2+}-mobility in a ventricular myocyte.

We have designed a, to our knowledge, novel method for measuring D_{CaSR}, without using Fluo-5N loaded into the SR. This avoids the possibility of the fluorophore ($K_{Ca} \approx 0.4$ mM) (9) artifactually enhancing luminal Ca^{2+}-mobility through its action as a mobile Ca^{2+}-buffer. Our method involves draining Ca^{2+} slowly from the SR by opening RyRs at one end, using a local exposure to caffeine. The drainage rate is estimated by then applying caffeine to the rest of the SR, after a given time interval, and measuring the residual Ca^{2+} released, using a cytoplasmic Ca^{2+}-fluorophore (Fluo-3). The technique has allowed us to estimate D_{CaSR} in both rat and guinea pig ventricular myocytes. Interestingly, these particular cells cannot be loaded reliably with the SR dye, Fluo-5N (15); so this method is the only one available for measuring their D_{CaSR}. It appears to be low, equal to or even lower than estimates of cytoplasmic Ca^{2+}-mobility. Possible reasons for the discrepancy between our measurement of D_{CaSR} and the high values suggested previously are considered. We use mathematical modeling to investigate the potential consequences of low D_{CaSR} for the cycling of SR Ca^{2+} within a sarcomere and for the localization of luminal Ca^{2+}-events such as Ca^{2+}-blinks and other nanoscopic or microscopic SR phenomena.

METHODS

Solutions

Normal Tyrode (NT) contained 130 mM NaCl, 4.5 mM KCl, 20 mM Hepes, 2 mM $CaCl_2$, 1 mM $MgCl_2$, 11 mM glucose. 0Na0Ca Tyrode contained 120 mM *N*-methyl-D-glucamine (NMDG), 4.5 mM KCl, 20 mM Hepes, 1 mM $MgCl_2$, 0.5 mM EGTA, 11 mM glucose. 0Na10Ca Tyrode was as for 0Na0Ca, but with 10 mM $CaCl_2$ and 110 mM NMDG and no EGTA. Solution pH was adjusted to 7.4 with 5 M HCl (0Na0Ca/0Na10Ca) or 4 M NaOH (NT). Cyclopiazonic acid (CPA), caffeine, and tetracaine (Tet) were obtained from Sigma (Dorset, UK).

Cell preparation

Rat and guinea pig ventricular myocytes were isolated by a combination of enzymatic (Roche Blendzyme III for rat (Roche, Basle, Switzerland); Sigma collagenase for guinea pig) and mechanical dispersion (16,17). Cells in Dulbecco's modified Eagle's medium were loaded (10 min) with the AM-ester of Fluo-3 (stock in DMSO; final concentration 10 μM) or, in one experimental series, carboxy-SNARF-1 (10 μM). Cells were superfused at 37°C in a chamber mounted on a DM-IRBE microscope (Leica, Wetzlar, Germany). Cell adhesion was improved by pretreating the chamber with poly-L-lysine (0.01%). Pacing (to load SR) was achieved by field stimulation through two platinum wires in the chamber.

Confocal imaging and analysis

Cells were imaged confocally (Leica TCS-NT). Fluo-3 was excited (488 nm argon laser), and fluorescence emission (>515 nm) was collected by a photomultiplier tube (for dye calibration, see Fig. S1 in Supplementary Material, Data S1). Images in xyt-mode were acquired at 256 × 256 pixels every 1.1 s. Line scans along the long axis of a myocyte were acquired at 256 pixels every 2.5 ms. In-house ImageJ (National Institutes of Health, Bethesda, MD) macros were used for background-subtraction and myocyte-edge detection. Fluorescence was averaged in regions of interest (ROIs) and then normalized to diastolic fluorescence (F_0). Data are presented as mean ± SE.

Protocol for Ca^{2+}-loading and stabilizing SR

Before experiments, myocytes were initially paced electrically (2 Hz) for up to 2 min to load the SR with Ca^{2+}. Sarcolemmal Ca^{2+}-flux (through L-type channels and Na^+/Ca^{2+} exchange) was then eliminated by halting stimulation and superfusing myocytes with Na^+-free Ca^{2+}-free solution (0Na0Ca) (9,18,19). This did not alter resting $[Ca^{2+}]_i$, but it initially triggered Ca^{2+}-waves (Fig. 1 *A*). These suggested fluctuations in $[Ca^{2+}]_{SR}$, which would complicate our analysis. We therefore blocked SERCA by including 10 μM CPA in 0Na0Ca (''stabilizing solution'', SS), and we attenuated SR Ca^{2+}-leak (which blocked the occurrence of Ca^{2+}-waves) with 0.3 mM or 2 mM Tet. In the presence of SS + Tet, steady-state F/F_0 decreased by 25%, within 2 min, following a similar time course in both doses of Tet (Fig. 1 *B*). This fall in fluorescence was not due to quenching of Fluo-3 fluorescence by Tet or CPA, as it was absent in cells AM-loaded with 100 μM BAPTA, an intracellular Ca^{2+}-buffer that clamps $[Ca^{2+}]_i$ (Fig. 1 *C*). Cells stabilized in SS + Tet were used for the main experimental work. Once experiments performed in SS were completed, cells were superfused in NT again. This was used to correct for dye leakage by fixing F/F_0 at 1.0 in NT at steady state ($[Ca^{2+}]_i$ = 100 nM).

Measuring total SR Ca^{2+}-content

Total SR Ca^{2+} ($[Ca^{2+}]_{SRT}$; free + buffered) was estimated by superfusing Tet-free SS containing 10 mM caffeine (to activate maximally RyR channel opening) (20) and then measuring the peak rise of $[Ca^{2+}]_i$ (with Fluo-3; Fig. 2 *A*). Superfusion details are given in the next section. Although the fluorescence rise was transient, further caffeine challenges induced no additional Ca^{2+}-release (even after six consecutive caffeine episodes), confirming that the caffeine-sensitive store had been discharged completely and that SERCAs were fully inhibited by CPA. The recovery of $[Ca^{2+}]_i$ observed in caffeine (Fig. 2 *A*) is most likely caused by Ca^{2+}-extrusion from the cell on PMCA (plasmalemmal Ca^{2+}-ATPase) (19), as recovery was reversibly inhibited by raising superfusate $[Ca^{2+}]$ to 10 mM (Fig. 2 *B*), a maneuver known to inhibit the pump (19,21).

Some experiments required estimating $[Ca^{2+}]_{SRT}$ with a caffeine challenge immediately after a period of Tet superfusion. This was possible, as the inhibitory effects of Tet on RyR channels and the SR Ca^{2+} leak are fast (<3 s) and reversible (22,23). This was confirmed in this work from measurements of Ca_i^{2+} in the absence of CPA, showing that resting F/F_0 reversibly decreased by 19.5% ± 1.7% with a half-time of 2.7 ± 0.3 s on 0.3 mM Tet application and removal ($n = 5$; data not illustrated), consistent with rapid and reversible attenuation of SR Ca^{2+} leak. A slow Tet washout

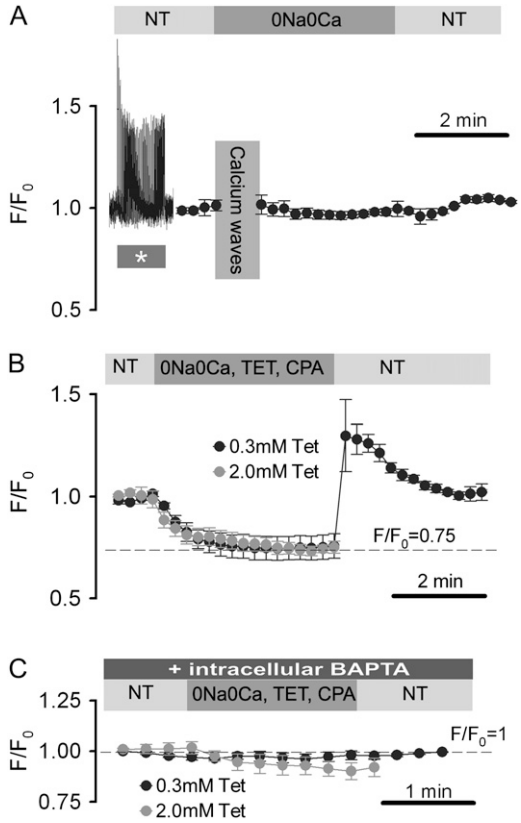

FIGURE 1 Protocol for stabilizing SR Ca^{2+} load. Rat myocytes. (*A*) Fluo-3 fluorescence (F/F_0) was measured in cells paced at 2 Hz in NT, and then superfused with 0Na0Ca medium (fluorescence normalized to diastolic levels in NT). Ca^{2+}-waves were observed in the first 2 min in 0Na0Ca. After waves ceased, diastolic F/F_0 was ~1. (*B*) In 0Na0Ca solution with SERCA inhibited by 10 μM CPA (stabilizing solution, SS), RyRs were dose-dependently inhibited by 0.3 or 2 mM Tet. Inclusion of Tet in SS-superfusate blocked Ca^{2+}-waves. At both doses of Tet, resting F/F_0 stabilized (at a 25% lower level) with a half-time of ~36 s. Cells stabilized in SS + Tet were then used for the main experiments. (*C*) The reduction of resting F/F_0 observed in the presence of SS + Tet was absent in rat cells preloaded with 100 μM BAPTA-AM. (*A–C*) Mean of 7–10 cells.

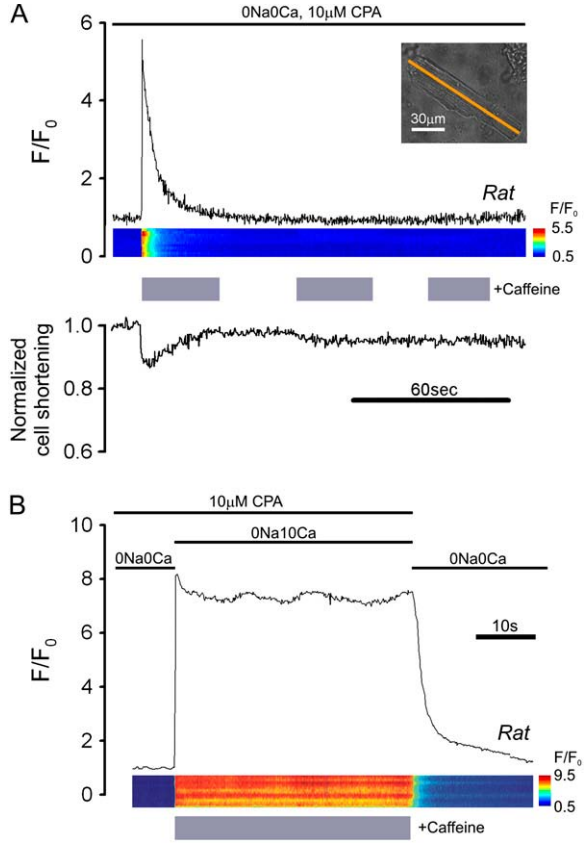

FIGURE 2 Mobilizing SR Ca^{2+} with caffeine. (*A*) Rat myocyte, AM-loaded with Fluo-3 and initially paced at 2 Hz in NT was then superfused with 0Na0Ca medium containing 10 μM CPA (stabilizing solution, SS), interspersed with three 30-s episodes of SS + 10 mM caffeine. (*Upper panel*) time course for F/F_0 averaged along a longitudinal line scan (*inset* indicates position of line scan axis); (*middle panel*) F/F_0 line scan; (*lower panel*) cell shortening. The first caffeine exposure mobilizes all SR Ca^{2+}. (*B*) Different rat myocyte exposed to SS containing 10 mM caffeine and 10 mM $[Ca^{2+}]_o$; note lack of Ca_i^{2+}-recovery, suggesting block of sarcolemmal PMCA. Final recovery in 0Na0Ca (with zero CPA) is attributable to SERCA and PMCA activity.

might be expected to reduce subsequent RyR activation by caffeine, and thus the mobilization of SR Ca^{2+}. It is notable, therefore, that pretreating cells with 0.3 mM or 2 mM Tet for 2 min did not attenuate the caffeine-induced rise of Ca_i^{2+} (measured in Tet-free SS), again consistent with rapid Tet washout. After 2 min pretreatment with SS + 0.3 mM Tet, the caffeine-evoked peak F/F_0 was 5.0 ± 0.4 (fluorescence-rise normalized to resting fluorescence in NT solution; $n = 8$); after 2 min pretreatment with SS + 2 mM Tet, $F/F_0 = 5.6 \pm 0.2$ ($n = 7$); after 2 min pretreatment with SS + zero Tet, $F/F_0 = 4.9 \pm 0.7$ ($n = 6$).

Localizing the caffeine exposure

Rapid caffeine exposure was performed using a dual-microperfusion apparatus (16,17,24,25), which can switch between solutions in <1 s. The device releases two microstreams from a double-barreled square-bore pipette, maintaining a sharp interstream boundary (<10 μm) due to high flow (1–2 mL/min) (16,25). The width of a single microstream (~300 μm) is sufficient to ensure that a whole myocyte, oriented at right angles to the flow, can be exposed uniformly to a solution held in one of the barrels. In this way, a myocyte could be uniformly exposed to a caffeine-containing solution. When required, a myocyte was regionally exposed to the drug by positioning the interstream boundary such that ~25% of the cell length was enveloped by the caffeine microstream, whereas the rest of the cell was exposed to a caffeine-free microstream. To visualize the boundary optically, one microstream also contained 10 mM sucrose, which itself had no effect on Ca^{2+}-signaling (16).

During partial exposure of a myocyte to caffeine, the drug's high membrane permeability (20 μm/s (26)) will ensure that its intracellular compartmentalization is similar to that imposed extracellularly. Caffeine, as a solute of molecular mass 200 Da, is expected to diffuse at ~50 $\mu m^2/s$ (estimated from Swietach and Vaughan-Jones (17)). For a 120-μm-long myocyte exposed proximally along 25% of its length to 10 mM caffeine, steady-state $[caffeine]_i$ at the distal end of the cell is expected to be <20 nM. $[caffeine]_i$ will fall to 1% (0.1 mM) within 6 μm of the midpoint of the microstream boundary (see Fig. S2 in Data S1 for the solution to a mathematical model of intracellular caffeine diffusion during partial extracellular exposure). Since the half-maximal caffeine dose for RyR channel opening in intact cells is 2–3 mM (27), the sharp compartmentalization of $[caffeine]_i$ will translate into a sharp compartmentalization of caffeine-induced RyR channel opening. Due to low cytosolic Ca^{2+}-mobility, the spread of Ca_i^{2+} will exceed the $[caffeine]_i$ profile by only 7% of cell length (see Appendix 1).

RESULTS

Estimating SR Ca^{2+}-leak

When SERCA is inhibited (for example, with CPA), SR-membrane leakage slowly depletes the SR (18). As described later, the leakage must be known when estimating D_{CaSR}. Leakage was assessed by assaying $[Ca^{2+}]_{SRT}$ with caffeine at various times after switching a cell into SS. Fig. 3, *A* and *B*, shows specimen confocal longitudinal line scan recordings of $[Ca^{2+}]_i$ (rat myocytes), indicating that caffeine-induced Ca^{2+}-release was smaller after 4 min than after 1 min, consistent with SR leakage depleting $[Ca^{2+}]_{SRT}$. Data pooled in Fig. 3 *C* indicate a time constant of ~200 s for the decline with 0.3 mM Tet but a much slower decline with 2 mM Tet. Fig. 3 *Cii* shows that the decline was paralleled by a similar fall in the peak contracture (Fig. 3, *A* and *B*) that coincided with SR Ca^{2+}-release. A comparable rate of rundown of $[Ca^{2+}]_{SRT}$ in 2 mM Tet was also observed in guinea pig myocytes (Fig. 3 *Ci*). We conclude that Tet dose-dependently reduces SR-membrane leakage.

Experimental protocol for measuring D_{CaSR}

A rat myocyte was positioned within a stream of SS plus 0.3 mM Tet, emerging from one barrel of a dual-microstream apparatus (Fig. 4 *A*; configuration 0). The other stream contained 10 mM caffeine in Tet-free SS. The interstream boundary was quickly (<1 s) moved (Fig. 4 *A*; configuration 1), exposing one end of the cell (proximal end) to caffeine (24.0% ± 1.3% and 23.0% ± 3.0% of the length in rat and guinea pig, respectively; $n = 87$ and 24). This resulted in proximal SR Ca^{2+}-release which was measured (as F/F_0) over the proximal 20% of the line scan (ROI-P, Fig. 4 *A*). After 30 s (Fig. 4 *Bi*), the solution boundary was readjusted, exposing the whole cell to caffeine (Fig. 4 *A*; configuration 2). There was now a local SR Ca^{2+}-release from the remainder of the cell (Fig. 4 *Bi*), which was measured (as F/F_0) over the distal 20% of the line scan (distal ROIs; ROI-D; Fig. 4 *A*). This distal Ca^{2+} rise was frequently accompanied by a smaller, slower Ca_i^{2+} rise in the proximal region, caused by back diffusion of cytoplasmic Ca^{2+}. Ca^{2+}-release events from the SR were associated with cell contractures.

Thus localizing a cell's exposure to caffeine allows one to assess local $[Ca^{2+}]_{SRT}$. Fig. 4 *Bii* shows that, in a different cell, increasing the time period (to 4 min) before readjusting the interstream boundary resulted in a considerably smaller caffeine-induced Ca^{2+}-release from the distal end of the cell. Thus prolonged exposure of a proximal SR region to caffeine also empties the unexposed distal region. Although some of this emptying may be caused by Ca^{2+}-leakage across the distal SR-membrane (the *dashed line* indicates the predicted leakage), there may also be emptying via luminal Ca^{2+}-diffusion from distal to proximal SR regions, where Ca^{2+}

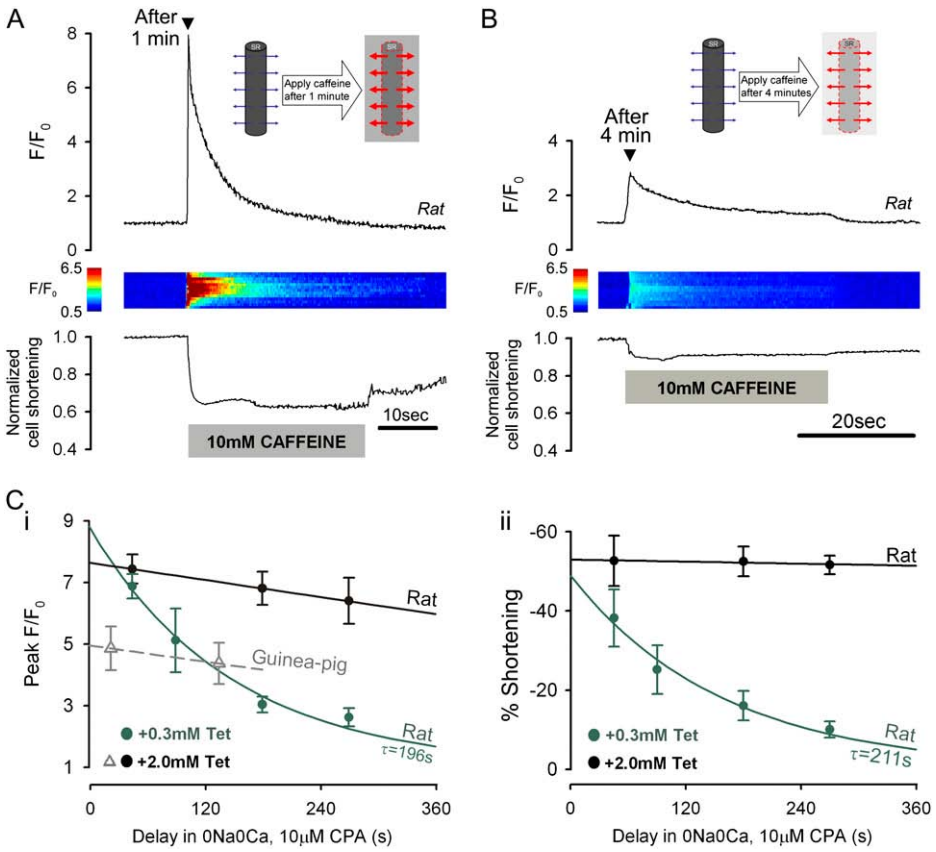

FIGURE 3 Assessing SR Ca^{2+}-leak. Myocytes paced at 2 Hz in NT were then superfused with SS containing 0.3 or 2.0 mM Tet. (*A*) After 1 min in SS + 0.3 mM Tet, rat myocyte was exposed to Tet-free SS + 10 mM caffeine for 30 s. (*Upper panel*) longitudinal line scan average for F/F_0; (*middle panel*) F/F_0 line scan (*y* axis normalized to cell length); (*lower panel*) cell shortening. (*B*) Different rat myocyte, exposed to caffeine after 4 min in SS + 0.3 mM Tet. Smaller Ca^{2+}-release is due to longer preceding period of SR-membrane Ca^{2+}-leakage. (*C*) (*i*) Peak F/F_0 during caffeine-exposure, measured after 1–6 min delay (normalized to F/F_0 at switch into SS) in rat myocytes in 0.3 mM (*green*) or 2 mM (*black*) Tet, and in guinea pig myocytes in 2 mM Tet (*gray*) (n = 5–10 cells/data-point). (*ii*) Cell shortening responses to caffeine in rat myocytes. Rundown of both F/F_0 and cell shortening gives time course of SR depletion caused by Ca^{2+}-leak.

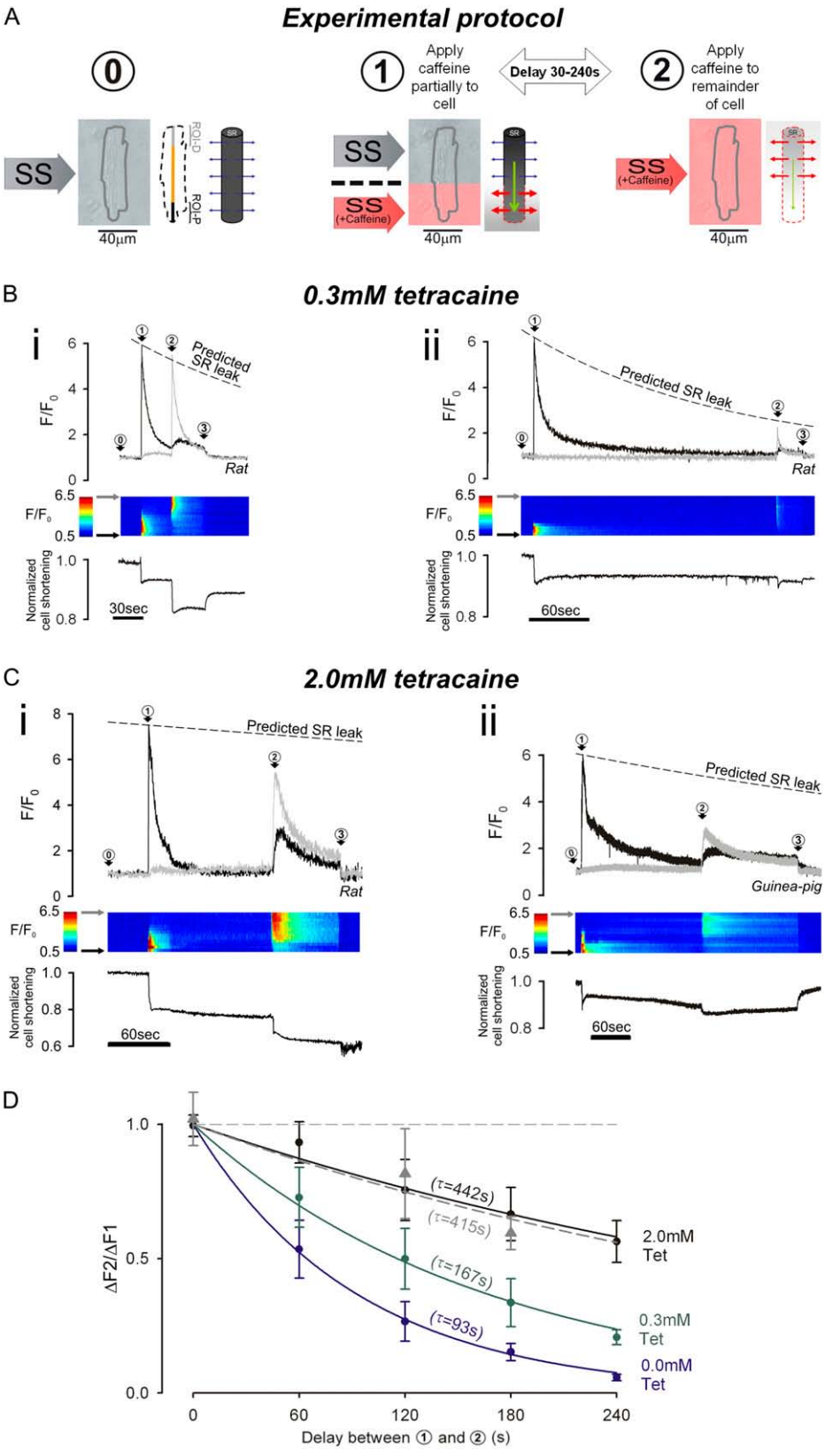

FIGURE 4 Measuring SR Ca^{2+}-mobility. Caffeine is used to estimate the decline of distal $[Ca^{2+}]_{SRT}$, while Ca^{2+} is being drained from the proximal end of SR. (*A*) Dual-microperfusion apparatus is used to deliver two solutions: SS (without Tet or with 0.3 or 2 mM Tet) and SS + caffeine (10 mM with no Tet). Myocyte is first bathed in SS + Tet (configuration 0). Throughout the experiment, intracellular Fluo-3 fluorescence (F/F_0) is averaged in two ROIs, each 20% of cell length, one positioned proximally (ROI-P) and one distally (ROI-D), at the ends of a line scan (see schematic diagram shown to the right of configuration 0). SS + caffeine is then applied to proximal end of myocyte to start SR-drainage (configuration 1); after a 30–240 s delay, SS + caffeine is applied to whole cell (configuration 2) to assess remaining SR Ca^{2+}-content. At the end of the experiment, cells are returned to 0Na0Ca, free of CPA, Tet, and caffeine (not illustrated, denoted by *arrow* 3 in *B* and *C*). (*B*) SS microstream (but not SS + caffeine microstream) contained 0.3 mM Tet. (*i*) Rat myocyte; delay of 30 s between configurations 1 and 2. (*Upper panel*) F/F_0-time course for $[Ca^{2+}]_i$ averaged in ROI-P (*black trace*) and ROI-D (*gray trace*). Dashed line shows predicted decline of caffeine-mobilizable Ca^{2+}-release because of SR Ca^{2+}-leak (from Fig. 3). (*Middle panel*) Longitudinal F/F_0 line scan (*y* axis normalized to cell length). (*Lower panel*) cell shortening. (*ii*) Rat myocyte; delay of 240 s between configurations 1 and 2. (*C*) SS microstream (but not SS + caffeine microstream) contained 2.0 mM Tet. (*i*) Rat myocyte; delay of 120 s between configurations 1 and 2. (*ii*) Guinea pig myocyte; delay of 180 s between configurations 1 and 2. (*D*) Ratio of distal fluorescence rise (configuration 2) to initial proximal rise (configuration 1), ΔF2/ΔF1, for different delay times. Rat myocytes with 2 mM Tet (*black*), 0.3 mM Tet (*green*), and zero Tet (*blue*). Guinea pig myocytes with 2 mM Tet (*gray*) (4–12 cells/data point). Time constants (τ) obtained from monoexponential fits.

escapes through caffeine-opened RyRs. This luminal diffusion was examined further by repeating the experimental protocol, but with 2.0 mM rather than 0.3 mM Tet, to inhibit most of the SR-membrane leak (Fig. 4 *C*). After a 2 min exposure of proximal SR to caffeine, the Ca^{2+}-content of the distal SR region again became depleted, but this was now clearly more than expected from SR-membrane leakage alone (*dashed line*). Reducing the SR leak with 2 mM Tet, therefore, reveals that exposure of proximal SR to caffeine can drain distal areas via luminal Ca^{2+}-diffusion.

Fig. 4 *D* plots the time course of decline of the distal SR Ca^{2+}-content during proximal caffeine exposure in the presence of 0, 0.3, and 2 mM Tet (from a total of 87 rat myocytes and 24 guinea pig myocytes). In all cases, the Ca^{2+}-content decreased, but more slowly at higher Tet concentrations, reflecting the reduced SR-membrane leak. In 2 mM Tet, SR-membrane leak is minimal, and the decline will be caused largely by spatial SR Ca^{2+}-diffusion from distal to proximal areas. Note that this rate of decline (in 2 mM Tet) was similar in both guinea pig and rat myocytes.

As shown in Fig. 5, local $[Ca^{2+}]_{SRT}$ can be assessed from the contracture during a local caffeine challenge. To check that Ca^{2+}-binding by Fluo-3, used in this work, did not affect the rate of local SR depletion, we monitored the decline of the distal contracture with caffeine after increasing periods of proximal caffeine exposure. It declined at the same rate irrespective of whether a cell was AM-loaded with Fluo-3 or with carboxy-SNARF-1, a fluorescent dye that does not bind Ca^{2+} (Fig. 5 *B*). Thus the presence of the Ca^{2+}-fluorophore does not affect the rate at which luminal Ca^{2+}-diffusion and Ca^{2+}-leak drains the SR.

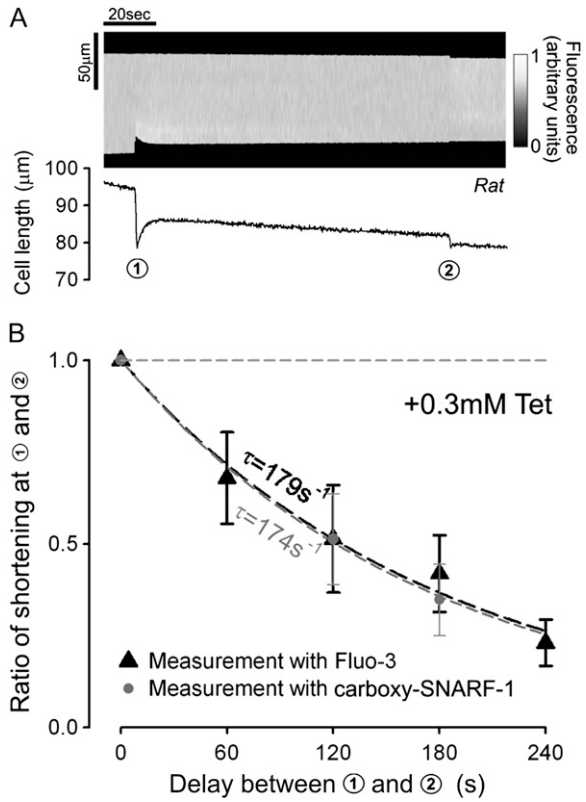

FIGURE 5 Distal SR depletion with proximal caffeine is unaffected by Fluo-3. (*A*) Myocyte AM-loaded with carboxy-SNARF-1, a non-Ca^{2+} binding fluorophore. Upper panel: fluorescence line scan (*y* axis shows cell length) used to monitor cell shortening (carboxy-SNARF-1 excitation at 514 nm, emission at 580 nm). (*Lower panel*) time course of cell shortening (derived from *upper panel*) in response to caffeine. Protocol of Fig. 4 was applied. Cell initially exposed to SS + 0.3 mM Tet. At circle 1, the proximal end of the cell exposed to SS + 10 mM caffeine; at circle 2 the whole cell exposed to SS + 10 mM caffeine. (*B*) Ratio of second/first shortening-event is plotted versus time delay between circles 1 and 2 in the presence of intracellular carboxy-SNARF-1 (*black*; $n = 8, 7$) or Fluo-3 (*gray*; $n = 6$–13). Time constants (τ) obtained from monoexponential fits. The presence of the Ca^{2+}-binding fluorophore, Fluo-3, does not affect the rate of decline of distal contraction (and hence distal SR-depletion) during proximal caffeine exposure.

Calculating D_{CaSR}: simple diffusion model

Rates of local SR-depletion were used to quantify D_{CaSR} by applying a simple one-dimensional (1-D) diffusion model of the SR, featuring both longitudinal Ca^{2+}-diffusion and lateral membrane Ca^{2+}-leak (Fig. 6 *Ai*):

$$\frac{\partial [Ca^{2+}]_{SRT}}{\partial t} = D_{CaSR} \times \frac{\partial^2 [Ca^{2+}]_{SRT}}{\partial x^2} - \lambda \times [Ca^{2+}]_{SRT}.$$

The model makes no assumptions about the cause of any deviation of Ca^{2+}-mobility from its high value in water ($D_{Ca} \approx$ 1000 $\mu m^2/s$) (28). SR-membrane leak is defined as the product of rate constant λ (estimated from Fig. 3 *Ci* for different Tet doses) and total SR Ca^{2+} content.

This definition of SR-membrane leak is in agreement with the monoexponential decline in SR content (Fig. 3 *Ci* and Bassani and Bers (18)) and allows for local variation in SR leak that can arise from SR depletion, driven by intra-SR Ca^{2+}-diffusion. The caffeine-induced rise in Fluo-3 fluorescence was converted to $[Ca^{2+}]_i$ and, after accounting for cytoplasmic (intrinsic + Fluo-3) buffering (29), to $[Ca^{2+}]_{SRT}$ (for full details, see Appendix 1). The time course of depletion of distal $[Ca^{2+}]_{SRT}$ by proximal caffeine (Fig. 4 *D*) was solved by best-fitting a single D_{CaSR} value in the diffusion model. Depletion can be fitted in this way because $[Ca^{2+}]_{SR}$ equilibrates relatively rapidly (~10 ms) with $[Ca^{2+}]_{SRT}$ (30), and the two parameters will be linearly related, given that the binding constant (3,30,31) of the principal luminal buffer, calsequestrin, is greater than or similar to $[Ca^{2+}]_{SR}$. Fitting results are shown in Fig. 6 *Aii*. The least-squares best-fit value for D_{CaSR} is low, 8–9 $\mu m^2/s$ and is similar in both rat and guinea pig myocytes. The same best-fit value is obtained for conditions of high or low SR leak (0.3 and 2.0 mM Tet, respectively), suggesting that the model makes adequate correction for this. Interestingly, when the influence of the leak is ignored (λ forced to equal 0), the predicted D_{CaSR} value is not unique. It increases with leak size and appears to be

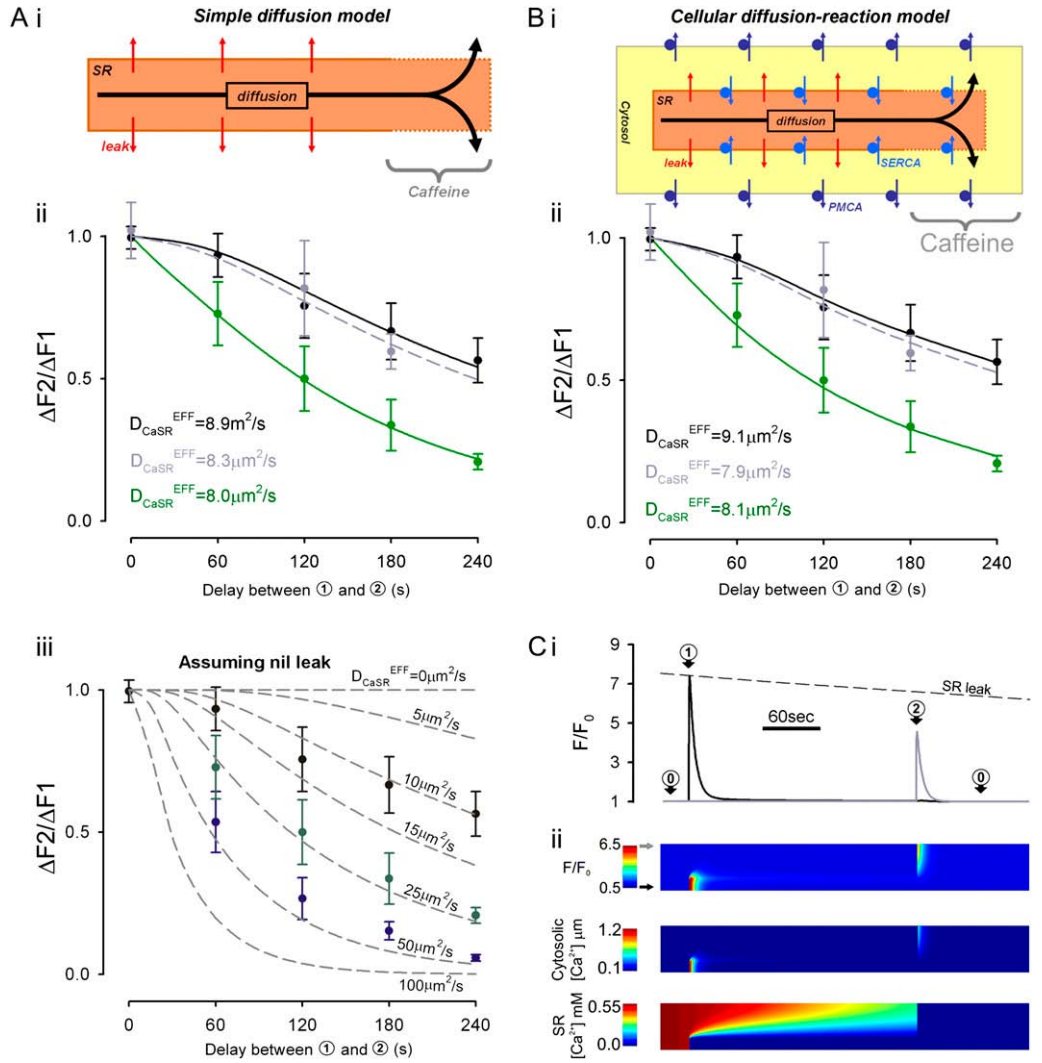

FIGURE 6 Quantifying D_{CaSR}. (*A*) (*i*) Schematic diagram of the simple Ca^{2+}-diffusion model, incorporating SR-membrane leak and proximal SR-exposure to caffeine (see Appendix 1). (*ii*) Best-fitting of diffusion model (SERCA activity = 0, simulating CPA-addition) to data in Fig. 4 *D* gives displayed values for D_{CaSR} (0.3 mM Tet, *green*; 2 mM Tet, *black*: rat myocytes; 2 mM Tet, *gray*: guinea pig myocytes). Note unique value for D_{CaSR} (8–9 $\mu m^2/s$). (iii) Best-fitting when SR Ca^{2+}-leak is ignored; note lack of unique value for D_{CaSR} (42, 23, and 10 $\mu m^2/s$ for rat myocyte data (Fig. 4 *D*) with 0, 0.3, and 2 mM Tet, respectively). (*B*) (*i*) Schematic diagram of diffusion-reaction model showing principal reaction elements (see Appendix 1). (*ii*) Displayed D_{CaSR}: best-fit values averaged between 0 and 240 s. (*Green*) rat, 0.3 mM Tet; (*black*) rat, 2 mM Tet; (*gray*) guinea pig, 2 mM Tet. Note similarity with D_{CaSR} values from *A*ii. (*C*) Output of cellular diffusion-reaction model simulating experimental protocol (Fig. 4). (*i*) Time course of F/F_0 from simulated line scan in proximal (*black*) and distal (*gray*) ROIs. (*ii*) Simulated line scans for F/F_0, $[Ca^{2+}]_i$ and $[Ca^{2+}]_{SR}$.

42 $\mu m^2/s$ in the absence of Tet. Thus accurate measurement of global D_{CaSR} requires a full correction for the effects of SR-membrane leak.

Calculating D_{CaSR}: mechanistic diffusion-reaction model

D_{CaSR} was quantified a second way, this time using a mechanistic, 1-D diffusion-reaction model (Fig. 6 *Bi*). This approach attempts to account for elements affecting both luminal and cytoplasmic Ca^{2+}, such as RyR-permeability, luminal and myoplasmic Ca^{2+}-buffers (including Fluo-3), and, where appropriate, the membrane transporters SERCA and PMCA. Parameters for these elements were derived either from the literature or from this work (see Appendix 1 and Table 1). The model best fits experimental data with a single Ca^{2+}-diffusion coefficient (D^{tort}_{CaSR}). This value is lower than its free aqueous value D_{Ca} because of SR tortuosity. The effective Ca^{2+}-diffusion coefficient (D_{CaSR}) in the SR is, however, reduced further because of luminal buffering by calsequestrin (3,31):

$$D_{CaSR} = D^{tort}_{CaSR} \times \left(1 + \frac{C_{csq} \times K_{csq}}{\left(K_{csq} + \left[Ca^{2+}\right]_{SR}\right)^2}\right)^{-1}. \quad (1)$$

TABLE 1 Model parameters

Symbol	Definition	Value	Reference
$[Ca^{2+}]_{i,0}$	Diastolic myoplasmic Ca^{2+} in NT	100 nM (75 nM in Tet)	(39,40,43,46)
$[Ca^{2+}]_{SR,0}$	Diastolic fully loaded SR Ca^{2+} in NT	520 μM (700 μM in Tet)	(3,31,46)
v_{cell}	Total cell volume	33 pL	(43,47)
v_{SR}	Total SR volume	3.5% of V_{cell}	(1,48)
v_{myo}	Total nonmitochondrial volume	65% of V_{cell}	(1,43,48)
ρ_{SL}	SL surface area/volume ratio	0.89 μm^{-1}	(47,49)
ρ_{SR}	SR surface area/volume ratio	1.19 μm^{-1}	(1,48)
L	Cell length	120 μm (rat); 113 μm (g-p)	Measured
E	% SR mobilized during partial caffeine exposure	24% (rat); 23% (g-p)	Measured
k_{leak}	SR leak rate constant	See text	Fig. 2
k_{rel}	Caffeine-evoked Ca^{2+}-release rate constant	9 s^{-1}	(50)
V_S^{max}	Maximum rate of SERCA	100 μM s^{-1}	Estimated*
K_S^f	Ca_i^{2+} affinity of SERCA (forward)	0.246 μM	(43)
K_S^r	Ca_i^{2+} affinity of SERCA (reverse)	1.7 μM	(43)
n_S	Hill cooperativity of SERCA	1.787	(43)
V_P^{max}	Maximum rate of PMCA in 0Na0Ca media (estimated from relaxation time constant)	30.0 μM s^{-1} (rat); 25.4 μM s^{-1} (g-p)	e.g., Fig. 1 *A*
K_P	Ca_i^{2+} affinity of PMCA	0.5 μM	(43)
J_{bal}	SL Backflux to balance PMCA and stabilize $[Ca^{2+}]_i$	Adjustable	
C_{buf}	Cytoplasmic (fast) buffer concentration	175 μM	(29)
K_{buf}	Cytoplasmic (fast) buffer equilibrium constant	0.59 μM	(29)
C_{CSQ}	Calsequestrin buffer concentration (estimated from rise in total cytosolic Ca^{2+} during caffeine exposure)	4.4 mM (rat); 2.3 mM (g-p)	Estimated*
k_{CSQ}^{off}	Calsequestrin Ca^{2+} off-rate	109 s^{-1}	(30)
K_{CSQ}	Calsequestrin Ca^{2+} binding constant	0.63 mM	(3,31)
C_{Fluo}	Fluo-3 buffer concentration	25 μM	Data S1
K_{Fluo}	Fluo-3 buffer Ca^{2+} affinity	832 nM	Data S1
K_{Fluo}^{off}	Fluo-3 buffer Ca^{2+} off-rate	100 s^{-1}	Assumed
D_{Cai}	Cytosolic effective Ca^{2+} mobility (absence of Fluo-3)	15 $\mu m^2/s$	(7,39–41)
D_{Fluo}	Fluo-3 diffusion coefficient	25 $\mu m^2/s$	(39,40)
D_{Caff}	Caffeine diffusion coefficient	50 $\mu m^2/s$	Data S1
P_{Caff}	Caffeine permeability constant	9 μm/s	(26)

SL, sarcolemma; SR, sarcoplasmic reticulum; r, rat; g-p, guinea pig.
*P. Swietach, K. W. Spitzer, and R. D. Vaughan-Jones, unpublished.

C_{csq} and K_{csq} are the total concentration and Ca^{2+}-binding constant for calsequestrin, respectively. The least-squares best-fits of the model to the experimental data are shown in Fig. 6 *Bii*. These fits are very similar to those achieved using the simple diffusion model (Fig. 6 *Aii*). In both cases, the goodness of fit was high (sum of squares < 0.01). Because of luminal buffering, the effective D_{CaSR} in the model will vary with $[Ca^{2+}]_{SR}$, and so the value quoted for each curve in Fig. 6 *Bii* has been time-averaged over the whole period of local SR depletion to produce a mean for the experiment. This value is again low (7.9–9.1 $\mu m^2/s$) and is independent of the size of prevailing SR-membrane leak. The value is also similar in both rat and guinea pig cells. The confidence interval for our D_{CaSR} estimate can be approximated by best fitting data within their mean $\pm$ SE. This interval was ± 4.4 and ± 3.6 $\mu m^2/s$ for rat and guinea pig myocytes, respectively.

A final cross-check was made for the experimental estimates of D_{CaSR}. If the Ca^{2+}-diffusion models used in the analysis are reliable, D_{CaSR} estimated during longitudinal SR-depletion with proximal caffeine should be the same, irrespective of where the depletion in the distal SR is estimated. We therefore positioned two ROI-Ds at different known distances downstream from the initial proximal area of caffeine exposure (where ROI-P was positioned). When the whole SR was eventually exposed to caffeine (configuration 2 of Fig. 4 *A*), the rise of Ca_i^{2+} in each ROI-D could be used to estimate D_{CaSR}, as described previously. ROI-D1 was positioned near the middle of the cell, such that its near border was at the cell's center, whereas ROI-D2 was positioned at the extreme distal end of the cell (this was the default position for ROI-D used in all other experiments). When best-fitted by our diffusion-reaction model, mean D_{CaSR} estimated using ROI-P in combination with ROI-D1 was 7.2 $\mu m^2/s$ ($n = 87$), which is similar to the estimate obtained using ROI-P in combination with ROI-D2 (8.6 $\mu m^2/s$; $n = 87$), confirming the validity of the analytical technique. We preferred to use the more extreme ROI-D measurements for general analysis, as these exhibited the better signal/noise ratio for SR Ca^{2+}-release (a larger Fluo-3 fluorescence increase), thus providing a more accurate estimate of SR Ca^{2+}-mobility.

Fig. 6 *C* shows a model simulation of an experiment on a rat ventricular myocyte, demonstrating that proximal caffeine

application is predicted to deplete distal SR regions by an amount very similar to that assessed experimentally (Fig. 4 *D*). We conclude that the low D_{CaSR} detected in our experiments here is consistent with the expected effects on Ca^{2+}-diffusion of SR tortuosity and luminal Ca^{2+}-buffering.

DISCUSSION

SR is continuous, and global D_{CaSR} is low

We find that, in both rat and guinea pig ventricular myocytes, locally opening RyRs at one end of the SR can drain it slowly of Ca^{2+}, indicating a low SR Ca^{2+}-mobility of 8–9 $\mu m^2/s$. This remains true, even after natural Ca^{2+}-leakage across the SR membrane has been minimized with 2 mM Tet. Diffusion of Ca^{2+} down the SR, a distance of ~60 sarcomeres, is consistent with previous observations that, when Fluo-5N is loaded into the SR, both Ca^{2+}-ions and the fluorophore can, over minutes, access all luminal regions, including the nuclear envelope (9). SR lumen therefore appears to be continuous and to extend beyond individual sarcomeres, as also suggested from anatomical observations of nSR breaching the Z-line region (2).

Our low value for D_{CaSR} is a global average, which includes both jSR and nSR Ca^{2+}-mobility. It also refers to a partially mobilized SR ($[Ca^{2+}]_{SR} \approx 0.25$ mM). By extrapolation, D_{CaSR} in loaded SR ($[Ca^{2+}]_{SR} \approx 0.5$ mM) of guinea pig and rat would be 11–13 $\mu m^2/s$ (up to $[Ca^{2+}]_{SR} \approx 1$ mM, the $[Ca^{2+}]_{SR}$-dependence of D_{CaSR} is near linear; Eq. 1). It is of interest to compare it with global cytoplasmic Ca^{2+}-mobility, D_{Cai}. This latter parameter is difficult to quantify using Ca^{2+}-fluorophores because they act as mobile buffers, enhancing Ca^{2+}-mobility. However, a value for skeletal myoplasm (7), measured using radiotracers rather than Ca^{2+}-fluorophores, is 14 $\mu m^2/s$ at 21°C. At 37°C this will be higher, ~20 $\mu m^2/s$ (28). The value is similar to estimates of D_{Cai} in neurons (16 $\mu m^2/s$; fluorophore corrected) (32) and similar to the value predicted in the absence of fluorophore by our cardiomyocyte diffusion-reaction model (16 $\mu m^2/s$ at 37°C). Global D_{CaSR} is therefore likely to be even lower than D_{Cai}.

Ca^{2+}-mobility in water, D_{Ca}, is 1000 $\mu m^2/s$ at 37°C (7,28). Mobility in luminal SR is therefore reduced by about two orders of magnitude. Diffusion-reaction modeling of our experimental data (Fig. 6 *D*) suggests that one order of magnitude reduction is likely to be due to SR tortuosity (see Appendix 1), whereas the other can be attributed to luminal Ca^{2+}-buffering. Assuming a similar total nSR and jSR volume (2), the jSR concentration of calsequestrin, the principal luminal buffer, is between 6 mM (3) and 28 mM (31), and K_{csq} for Ca^{2+} is ~0.6 mM (3,31), a value close to $[Ca^{2+}]_{SR}$ in loaded SR, thus ensuring a maximal Ca^{2+}-buffering capacity. As calsequestrin is poorly mobile (molecular mass of 45 kDa), it will significantly attenuate luminal Ca^{2+}-mobility.

Our estimate of D_{CaSR} (8–9 $\mu m^2/s$) is nearly 10-fold lower than a previous measurement (9) (60 $\mu m^2/s$ at 20°C approximates to 84 $\mu m^2/s$ at 37°C (28)), obtained using luminal Fluo-5 N to measure SR Ca^{2+}-movement directly. It is not immediately apparent why the two estimates would differ so dramatically. Species differences (rabbit versus the guinea pig and rat here) are an unlikely explanation as, among the three cells, SR volume, and Ca^{2+}-content are believed to be similar (18). Furthermore, revising the earlier mobility measurement to the higher temperature of 37°C only accentuates the discrepancy (28). As mentioned already, the previous use of Fluo-5N for direct measurement of $[Ca^{2+}]_{SR}$ may have enhanced D_{CaSR}, but running our diffusion-reaction model suggests the effect would be by <2%, given the dye's low luminal concentration (50–100 μM (9)) compared with calsequestrin and $[Ca^{2+}]_{SR}$. Thus although Ca^{2+}-fluorophores like Fluo-3 and Fura-2 significantly affect cytoplasmic Ca^{2+}-mobility, the same is unlikely to be true for the effect of Fluo-5N on luminal Ca^{2+}-mobility (providing $[Ca^{2+}]_{SR} \gg$ [Fluo-5N]).

Unlike the previous work, we did not measure $[Ca^{2+}]_{SR}$ directly, but inferred it from local Ca^{2+}-release with caffeine. Indeed, direct $[Ca^{2+}]_{SR}$ measurements in rat and guinea pig ventricular myocytes were not an option, as reliable SR-loading of Fluo-5N in these cells has not so far been achieved (15). There is, therefore, the possibility of errors in our own work. The use of rapid caffeine application to assess $[Ca^{2+}]_{SRT}$ has, however, been well validated (18,29,31), as has the use of dual microperfusion to localize extracellular solutes with high precision (16,24,25). Due to caffeine's high membrane permeability (26), intracellular caffeine compartmentalization will also be similar to the extracellular compartmentalization imposed by dual microperfusion (see Methods and Data S1). Although caffeine-application gauges $[Ca^{2+}]_{SRT}$ rather than $[Ca^{2+}]_{SR}$, the two levels equilibrate in ~0.01 s (calsequestrin unloading rate constant = 109 s^{-1} (30)) and will thus decline in synchrony during local drainage, as jSR and nSR are interconnected throughout the cell.

One possible source for the discrepancy is the correction for SR membrane leakage. Our estimates of the time constant of Ca^{2+}-leakage (in low or zero Tet) are in agreement with previous estimates (18) and would produce 45% SR depletion during the time required to measure luminal Ca^{2+}-diffusion (~2 min). Although SR leakage was accounted for in this work, no leakage was apparent in the earlier determination of D_{CaSR} (see Fig. 7 of Wu and Bers (9)). Given that SR leakage is known to occur, this may indicate some residual SERCA activity in the earlier work (9), despite a 90 s exposure to 5 μM thapsigargin. It is notable that failure to account for leakage in this work results in artifactually high values for D_{CaSR} (up to ~42 $\mu m^2/s$; Fig. 6 *Aiii*). We show, in Fig. S3 in Data S1, that it may also lead to an overestimate of D_{CaSR} using the experimental protocol adopted in the earlier work. If so, D_{CaSR} may be low in all three species. Alternatively, rabbit ventricular myocytes may be unusual in exhibiting a high luminal Ca^{2+}-mobility.

Functional consequences of low D_{CaSR}: microscopic localization of SR Ca^{2+}-signaling

Although the SR lumen appears continuous throughout the ventricular myocyte, this need not imply functional continuity. A low global value for D_{CaSR} means that local displacements of $[Ca^{2+}]_{SR}$ will not necessarily be transmitted to other regions, particularly if they are rapid and transient. This can be illustrated in our diffusion-reaction model (Fig. 7) by locally increasing RyR permeability to release Ca^{2+} along a 2 μm stretch of SR (roughly equivalent to Ca^{2+}-release from a single sarcomere) and computing $[Ca^{2+}]_{SR}$ after 250 ms. If global D_{CaSR} in the model is set to a high value (>60 $\mu m^2/s$), Ca^{2+}-release (in the presence of local reuptake by SERCA) is associated with only a modest local fall of $[Ca^{2+}]_{SR}$, as Ca^{2+} drawn diffusively from adjacent SR regions (and hence from adjacent sarcomeres) limits the local depletion. As a result, an extended length of lumen becomes significantly depleted (9 μm of lumen, at 5% depletion threshold, with $D_{CaSR} = 300\ \mu m^2/s$ and 7 μm with $D_{CaSR} = 60\ \mu m^2/s$; Fig. 7). Thus a localized Ca^{2+}-release is predicted to produce a more generalized SR depletion.

In contrast, when global D_{CaSR} is set to the value measured experimentally (9 $\mu m^2/s$), Ca^{2+}-release is associated with a considerably larger fall of $[Ca^{2+}]_{SR}$ but one that is more localized spatially (5% depletion in <4 μm of lumen; Fig. 7). Ca^{2+} is no longer drawn so extensively from adjacent regions (i.e., from adjacent sarcomeres), thereby preserving their integrity. Under these circumstances, local control of SR Ca^{2+}-release is complemented by a local control of $[Ca^{2+}]_{SR}$. Although the above modeling is simplistic (it does not, for example, reproduce the real geometry within an SR release site), it nevertheless implies that a low global value for both luminal and cytoplasmic Ca^{2+}-mobility may result in local cytoplasmic Ca^{2+}-microdomains being mirrored spatially by inverse luminal Ca^{2+}-microdomains—as indeed appears to happen for a Ca^{2+}-spark and its corresponding Ca^{2+}-blink (2,13), and for a cytoplasmic Ca^{2+}-wave and its corresponding wave of SR Ca^{2+}-depletion (13,33). Indeed, given that $[Ca^{2+}]_{SR}$ is suggested to be an important regulator of RyR channel gating (34), a low D_{CaSR}, by optimizing the amplitude and minimizing the spatial extent of local $[Ca^{2+}]_{SR}$ depletion, may play an important role in the luminal regulation of the Ca^{2+}-release process itself.

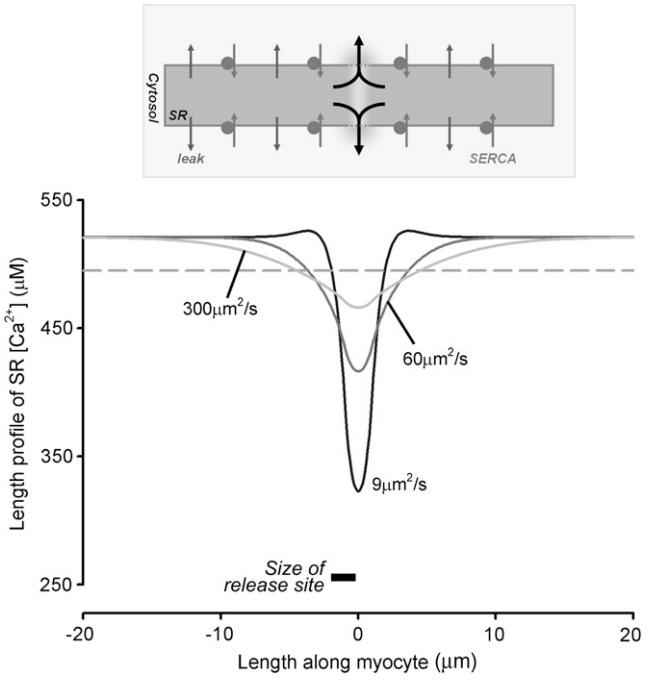

FIGURE 7 Effect of D_{CaSR} on longitudinal $[Ca^{2+}]_{SR}$ profile during simulated local Ca^{2+}-release. Diffusion-reaction model was run to simulate local SR Ca^{2+}-release (see Appendix 1). $[Ca^{2+}]_{SR}$ was calculated 250 ms after increasing SR-membrane permeability to 1.35 μM/s in a central 2 μm length of SR. This estimate of D_{CaSR} (9 $\mu m^2/s$) supports large and localized SR-depletion, with only small effects on adjacent luminal regions. Higher D_{CaSR} significantly depletes SR Ca^{2+} from regions beyond the release site. (*Dashed line*) 5% depletion threshold.

Changes in luminal Ca^{2+}-mobility may be relevant to recent reports of abnormal Ca^{2+}-signaling in ventricular myocytes. In one (34), increasing intra-SR Ca^{2+} buffering capacity with citrate or maleate was found to increase Ca^{2+} spark amplitude and duration. One possible explanation is an increase of D_{CaSR}, as these low molecular weight molecules will function as mobile Ca^{2+}-buffers within the SR lumen. An increased D_{CaSR} will finance a greater and more spatially diffuse Ca^{2+}-release, as illustrated in Fig. 7, and this may account for enhancement of the local Ca^{2+} spark. In a second report, the absence of calsequestrin from jSR in *Casq2*-null mice was found to be accompanied by an increased incidence of electrical arrhythmia (35). Results of this work predict that calsequestrin deletion, by reducing fixed luminal Ca^{2+}-buffers, would increase the effective D_{CaSR} (Eq. 1), again enhancing local Ca^{2+}-release. Such abnormal release may then contribute to the arrhythmic phenotype of *Casq2*-null mice (35). Conversely, calsequestrin overexpression would be expected to decrease D_{CaSR} (Eq. 1), which may play a role in the reduced spark frequency and Ca^{2+}-release observed recently in transgenic mice (36).

The low D_{CaSR} measured in this work has implications for models of Ca^{2+}-wave propagation during pathological conditions of Ca_i^{2+}-overload. Current hypotheses conflict, in that some assume a wave of $[Ca^{2+}]_{SR}$ depletion is coincident with the cytosolic Ca^{2+}-wave (13,33), whereas a recent hypothesis suggests an SR wave of luminal Ca^{2+}-loading that travels ahead of the cytosolic Ca^{2+}-wave (12). As discussed earlier, Eq. 1 predicts that, even when $[Ca^{2+}]_{SR}$ is as high as 1 mM, as may occur during the incidence of Ca^{2+}-waves, D_{CaSR} would still not be significantly greater than D_{Cai}, which tends to argue against the latter proposal. Finally, a low D_{CaSR} implies that conditions associated with spatially nonuniform Ca^{2+}-release within the cell, such as regional Ca_i^{2+} alternans, will, at times, be associated with significant spatial nonuniformity of $[Ca^{2+}]_{SR}$ (15,37).

Possible causes of low D_{CaSR}: local heterogeneity of SR Ca^{2+}-mobility

Although global D_{CaSR} is low, it is unlikely that Ca^{2+}-mobility is uniform throughout the SR, given its complex geometry and the heterogeneous distribution of luminal Ca^{2+}-buffers. It is therefore appropriate to ask which regional elements within the SR may limit the global movement of Ca^{2+}. One such element is likely to be jSR, which will have implications for SR Ca^{2+}-cycling within the sarcomere. The other may be the intersarcomeric portion of the nSR.

We deal first with jSR. During excitation-contraction coupling, after Ca^{2+}-release from jSR cisternae, Ca^{2+}-ion movement from nSR (the main site of Ca^{2+}-reuptake by SERCA) refills jSR within each cardiac cycle. In rabbit and canine myocytes, this refilling appears to occur with a time constant (τ) of 29 ms (2) and 98 ms (13), respectively, as derived from the recovery time course of a Ca^{2+}-blink (Fig. 8 *Aii*, *inset* for $\tau = 29$ ms). Such recovery will be a more direct measure of local jSR refilling than, for example, Ca^{2+} spark restitution, as the latter appears to depend on factors other than SR load, such as RyR refractoriness (38). If local cisternal refilling is by passive Ca^{2+}-diffusion, local $[Ca^{2+}]_{SR}$ recovery during a blink suggests that Ca^{2+}-mobility into or within jSR is low. Within each rabbit sarcomere, one jSR cisterna (diameter ≈ 0.6 μm) is supplied, on average, by four nSR elements (2) (Fig. 8 *Ai*; see Appendix 2 for derivation of geometry), with volume being distributed equally between jSR and nSR (2).

If one makes the simplifying assumption that, during an isolated Ca^{2+}-blink, the distal ends of the nSR elements are coupled to an infinite source of Ca^{2+} (because of diffusive coupling to quiescent elements of the SR and because of Ca^{2+}-uptake on SERCA), then local jSR refilling can be simulated by setting effective jSR Ca^{2+}-mobility to 1.8 $\mu m^2/s$ (for recovery $\tau = 29$ ms; Fig. 8 *Aii* and *iii*; see Appendix 2 for details). This is a very low value, consistent with restricted access to jSR from nSR and also consistent with the known high expression in jSR of calsequestrin (2,11). Thus, a very low, local D_{CaSR} may underpin the local luminal Ca^{2+}-flux required to refill jSR cisternae. But a predicted jSR Ca^{2+}-mobility of 1.8 $\mu m^2/s$ is significantly lower than the global value of D_{CaSR} measured in guinea pig and rat myocytes (8–9 $\mu m^2/s$) here. This may reflect a relatively high Ca^{2+}-mobility in non-jSR elements (i.e., in nSR), as implied in the SR-unit model (Fig. 8 *Ai* and Appendix 2). Indeed such an arrangement has already been proposed (2), as nSR is believed to be devoid of known Ca^{2+}-buffers, which would permit faster Ca^{2+}-diffusion (2,11).

A two-dimensional (2-D) model network of jSR-nSR elements (Fig. 8 *Bi*) with unbuffered Ca^{2+}-mobility in nSR and low, buffered Ca^{2+}-mobility in jSR (1.8 $\mu m^2/s$) can be used to predict the global value for D_{CaSR} (see Appendix 2 for details). Imposing zero-$[Ca^{2+}]$ at one end of the 2-D network (equivalent to tonically exposing one end of the SR to caffeine) predicts universal depletion, with an average D_{CaSR} of 8 $\mu m^2/s$ (Fig. 8 *Bii*), which is in agreement with the global value measured experimentally. Thus, if we assume heterogeneity of Ca^{2+}-mobility between jSR and nSR, as proposed previously, our experimentally determined value for D_{CaSR} would be sufficient to support local SR Ca^{2+}-signaling, as well as global luminal Ca^{2+} movement within the cardiac cell. The modeling implies that, at the nanoscopic level, luminal Ca^{2+}-diffusion will vary, being very slow in jSR but faster in nSR. The global Ca^{2+} diffusion rate through the combined SR elements will tend toward the lower of the two individual limits, as shown in Fig. 8 *Bii*.

What about intersarcomeric SR? The above modeling of luminal Ca^{2+}-diffusion takes no account of possible heterogeneity of Ca^{2+}-mobility within nSR itself. For example, it is possible that SR Ca^{2+}-diffusion is severely limited between adjacent sarcomeres (2), i.e., via intersarcomeric network SR (we call this *inSR*). Local Ca^{2+}-mobility for *inSR* may be significantly lower than for intrasarcomeric nSR, i.e., the part of the nSR that ramifies within each sarcomere and makes connection with jSR cisternae (we call this intrasarcomeric network *snSR*). Low Ca^{2+}-mobility for *inSR* would be consistent with the apparently sparse nature of *inSR* elements compared with the more densely arranged *snSR* elements (2). Subdividing nSR into *inSR* and *snSR* in our 2-D model network (Fig. 8 *Biii*) would have no effect on the predicted value for global D_{CaSR}, as the influence of the combined *inSR-snSR* would need to be identical to the original lumped nSR. In the simplest case, the subelements may be arranged in series, as shown in Fig. 8 *Biii*.

Analysis of the 2-D network indicates that the effective Ca^{2+}-mobility for a lumped nSR would be 110 $\mu m^2/s$ for a D_{jSR} of 1.8 $\mu m^2/s$ and a global D_{CaSR} of 8 $\mu m^2/s$ (see Appendix 2). Ascribing specific values to Ca^{2+}-mobility in the *inSR* or *snSR* subelements must await an anatomical description of their volume and tortuosity. But if Ca^{2+}-mobility for *inSR* were as low as for jSR (i.e., 1.8 $\mu m^2/s$), then the total nSR could be represented by a short *inSR* element with low Ca^{2+}-mobility coupled to a longer *snSR* element with high Ca^{2+}-mobility, where *inSR* is $\sim$1.5% of total nSR length (see Appendix 2). Thus, in effect, the *inSR* would occupy only a tiny fraction of total nSR volume, and so its limiting influence on global Ca^{2+}-mobility would not be large. In this way, effective Ca^{2+}-mobility in the whole nSR would still be 110 $\mu m^2/s$. At this time, subdividing local Ca^{2+}-mobility within the nSR is purely speculative. Furthermore, it takes no account of other regions of the SR/ER system, such as the nuclear envelope. As all these regions are interconnected (9), a comprehensive model of local Ca^{2+}-mobility will require detailed characterization of all these noncisternal elements.

We can now attempt to answer the question of which regional elements within the SR may limit the global diffusion of luminal Ca^{2+}. Assuming that the published recovery time for a Ca^{2+}-blink represents diffusive refilling of jSR, it seems likely that the effective Ca^{2+}-mobility in jSR is much lower than that averaged throughout the rest of the SR/ER. Because

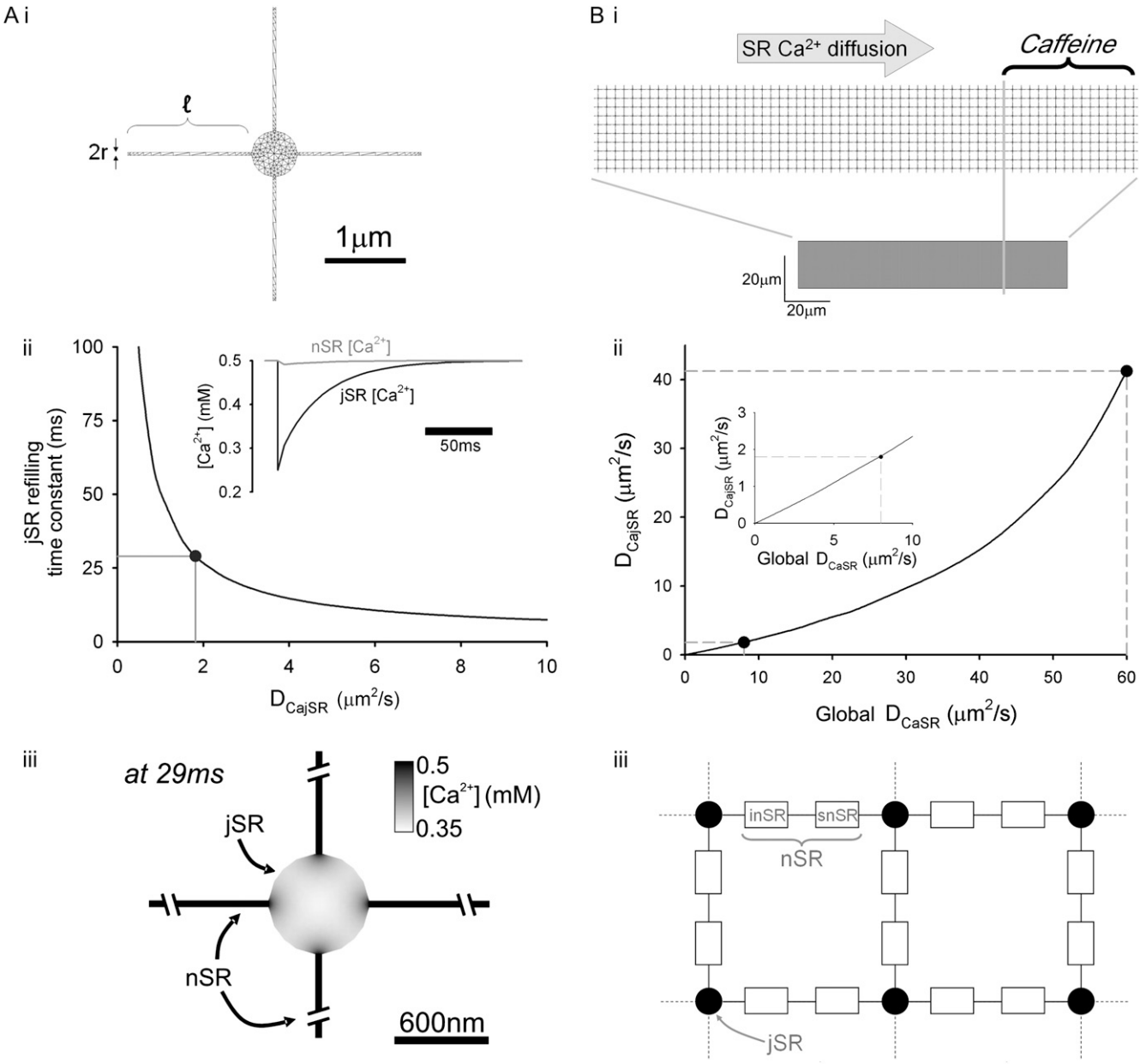

FIGURE 8 Modeling Ca^{2+}-diffusion in SR nanoarchitecture. (*A*) (*i*) 2-D geometry for a unit of sarcomeric SR (jSR-cisterna connected to four nSR-tubes) triangulated for diffusion modeling. (*ii*) To simulate jSR Ca^{2+}-recovery after local Ca^{2+}-release, $[Ca^{2+}]_{jSR}$ was set instantaneously to 0.25 (50% depletion), whereas $[Ca^{2+}]_{nSR}$ was set initially to 0.5 mM and the distal ends of the nSR elements were coupled to an infinite 0.5 mM Ca^{2+} source. The time constant (τ) of recovery of $[Ca^{2+}]_{jSR}$ was then derived for a range of jSR Ca^{2+}-mobility values (D_{CajSR}), with Ca^{2+}-mobility in nSR assumed to be 1000 $\mu m^2/s$. The predicted time courses of change for $[Ca^{2+}]_{jSR}$ and $[Ca^{2+}]_{nSR}$ are shown in the inset. Filled circle denotes $\tau = 29$ ms, which has been determined experimentally for rabbit SR Ca^{2+}-blinks. (*iii*) Spatial $[Ca^{2+}]_{SR}$ map after 29 ms of jSR-refilling for a D_{CajSR} of 1.8 $\mu m^2/s$. (*B*) (*i*) 63 × 10 SR units based on *Ai*, coupled into a 2-D network for simulating whole-SR during proximal caffeine exposure (see Appendix 2). (*ii*) Predicted relationship between global D_{CaSR} and D_{CajSR}. D_{CajSR} of 1.8 $\mu m^2/s$ (derived from normal Ca^{2+}-blink recovery rate) predicts a global D_{CaSR} of 8 $\mu m^2/s$, similar to the value measured experimentally. In contrast, a high global D_{CaSR} (60 $\mu m^2/s$) predicts a relatively high D_{CajSR} (41 $\mu m^2/s$), which would then predict an ultrafast Ca^{2+}-blink recovery τ of <1 ms (see *Aii*). (*Inset*) Close-up of D_{CaSR} range between 0 and 10 $\mu m^2/s$. (*iii*) Model of nSR/jSR unit featuring a minimal length nSR (0.65 μm), divided into *snSR* and *inSR*. Diffusion in the *inSR* is slower than in the *snSR* (see Appendix 2 for details).

jSR occupies around half of total SR volume (2), its limiting effect on global Ca^{2+}-mobility will be large. Effects of intersarcomeric nSR are more difficult to quantify, but, when lumped with the rest of the nSR, they probably limit global Ca^{2+}-mobility far less than does jSR.

Low D_{CaSR} and SR Ca^{2+}-scraps

The spatial uniformity of $[Ca^{2+}]_{SR}$ during Ca^{2+}-scraps, where global SR Ca^{2+}-release during an action potential appears to deplete both jSR and nSR elements, has led to suggestions for a high global value for D_{CaSR} (8). In contrast,

the recovery time course of a Ca^{2+}-blink, with little or no Ca^{2+} depletion in adjacent nSR, suggests D_{CaSR} is low (2). Observations on Ca^{2+}-scraps and Ca^{2+}-blinks are not necessarily contradictory. The Ca^{2+}-blink is measured as an isolated, low-probability event (2,14). Thus fast Ca^{2+} movement from neighboring, quiescent SR elements may minimize local nSR depletion, as observed experimentally ((2) and Fig. 8 *Aii*, *inset*). But during an action potential, the high spatial density of Ca^{2+}-blinks may prevent this from happening, leading to global nSR depletion accompanying the global Ca^{2+}-discharge from jSR. As suggested previously (2,13), the recoveries of $[Ca]_{jSR}$ during an isolated Ca^{2+}-blink and a global Ca^{2+}-scrap (8) are likely to occur via different mechanisms, the former being via simple Ca^{2+}-diffusion and the latter via active Ca^{2+}-reuptake on SERCA pumps. A low global D_{CaSR} need not, therefore, be inconsistent with spatially uniform Ca^{2+}-scraps. In contrast, a high rather than low global D_{CaSR} of, say, 60 $\mu m^2/s$ would, from Fig. 8, *Aii* and 8 *Bii*, predict ultrafast diffusive jSR refilling after an isolated Ca^{2+}-blink, with a time constant of <1 ms, which could not be resolved experimentally. The fact that localized Ca^{2+}-blinks recover with a much longer time constant of 29–98 ms (2,13) thus reinforces our own proposal for a low D_{CaSR}.

CONCLUSIONS

We conclude that global D_{CaSR} in guinea pig and rat ventricular myocytes is 8–9 $\mu m^2/s$, a low value that is, nevertheless, consistent with the demands of SR Ca^{2+}-cycling during excitation-contraction coupling. Low global Ca^{2+}-mobility in the SR raises the possibility of local luminal control. This may, for example, help to preserve global Ca^{2+}-stores during aberrant local SR-release and may represent an additional layer in the local control of Ca_i^{2+}-signaling, complementing that exerted through the couplon.

APPENDIX 1: ESTIMATING D_{CaSR}

Simple Ca^{2+} diffusion model

A 1-D diffusion model (Fig. 6 *Ai*) was solved for total SR $[Ca^{2+}]$ ($[Ca^{2+}]_{SRT}$) over a compartment (length = myocyte length) featuring a passive leak (rate constant λ) to obtain an estimate of D_{CaSR}:

$$\frac{\partial [Ca^{2+}]_{SRT}}{\partial t} = D_{CaSR} \times \frac{\partial^2 [Ca^{2+}]_{SRT}}{\partial x^2} - \lambda \times [Ca^{2+}]_{SRT}. \quad (A1)$$

In experiments, local $[Ca^{2+}]_{SRT}$ was probed using caffeine application and was deduced from the resulting rise in total cytosolic $[Ca^{2+}]$ (free + buffered, $[Ca^{2+}]_{iT}$), which, in turn, was derived from Fluo-3 fluorescence (F/F_0). To convert F/F_0 to $[Ca^{2+}]_{iT}$, it must first be converted to free cytosolic $[Ca^{2+}]$ ($[Ca^{2+}]_i$):

$$[Ca^{2+}]_i = \frac{F/F_0 \times K_{fluo} \times [Ca^{2+}]_{i,0}}{K_{fluo} + [Ca^{2+}]_{i,0} \times (1 - F/F_0)},$$

where $[Ca^{2+}]_{i,0}$ is diastolic $[Ca^{2+}]_i$ (75 nM in Tet and 100 nM in the absence of Tet; Fig. 1). $[Ca^{2+}]_{iT}$ is then estimated from $[Ca^{2+}]_i$ knowing the characteristics of intrinsic (29) and Fluo-3 buffering (details of Fluo-3 calibration and buffering are given in Fig. S1 in Data S1):

$$[Ca^{2+}]_{iT} = [Ca^{2+}]_i \times \left(1 + \frac{C_{buf}}{[Ca^{2+}]_i + K_{buf}} + \frac{C_{fluo}}{[Ca^{2+}]_i + K_{fluo}}\right).$$

To estimate initial $[Ca^{2+}]_{SRT}$ and the SR leak constant λ, Eq. A1 (without the diffusive term) was fitted to the time courses of SR-depletion shown in Fig. 3 (no net spatial SR-diffusion in these experiments). This gave initial $[Ca^{2+}]_{SRT}$ values in rat and guinea pig myocytes of 135 and 88 μM in units of cytosolic volume (equivalent to 2.5 and 1.6 mM expressed in units of SR volume). The leak constant λ was rat: 4.5×10^{-3} and 4.4×10^{-4} s^{-1} at 0.3 and 2 mM Tet, respectively; guinea pig: 8.3×10^{-4} s^{-1} at 2 mM Tet.

The experimental protocol for measuring D_{CaSR} consisted of measuring the rate of depletion of distal $[Ca^{2+}]_{SRT}$ during proximal caffeine exposure (Fig. 4). As pointed out in the Results section, this is a valid approach, as i), $[Ca^{2+}]_{SRT}$ will equilibrate rapidly with $[Ca^{2+}]_{SR}$ (nonbuffered SR Ca^{2+}) because the principal SR buffer, calsequestrin, has rapid binding/unbinding kinetics (30); and ii), $[Ca^{2+}]_{SR}$ and $[Ca^{2+}]_{SRT}$ are linearly related (hence Eq. A1 is linear) because the Ca^{2+}-binding constant of calsequestrin (K_{csq}) is $\geq [Ca^{2+}]_{SR}$. On the timescale of the our experiments here (30–240 s), $[Ca^{2+}]_{SRT}$ and $[Ca^{2+}]_{SR}$ can be amalgamated into one diffusion equation.

The protocol of proximal caffeine exposure (Fig. 4) was simulated by assuming a nonuniform initial concentration profile (Fig. 6 *Ai*): $[Ca^{2+}]_{SRT}$ in the proximal region was set to equal diastolic $[Ca^{2+}]_i$ (75 nM in Tet). In the experiments, the boundary of the locally mobilized SR was determined optically from the position of the interstream boundary (Fig. 4 *A*, configuration 1) where it intersected the myocyte (highlighted by including 10 mM sucrose in one of the microstreams (16)). The boundary position could be confirmed by measuring the half-maximal width of F/F_0-rise on proximal caffeine exposure. This half-maximal width spans beyond the caffeine-exposed region by 7% due to cytosolic Ca^{2+}-diffusion (estimated using a diffusion-reaction model, see below). Experimentally, the boundary position was at 24% ± 1.3% and 23% ± 3.0% of cell length in rat and guinea pig myocyte experiments, respectively. To derive D_{CaSR}, the time-dependent depletion of distal $[Ca^{2+}]_{SRT}$ (Fig. 4 *D*) was best-fitted with the model. Results of fitting are shown in Fig. 6 *Aii*.

Mechanistic Ca^{2+} diffusion-reaction model

Estimating D_{CaSR}

The compartments (myoplasm and SR) and fluxes featured in the 1-D diffusion-reaction model are shown in Fig. 6 *Bi*. The system consists of six equations describing diffusion (vector **D**) and reaction (vector **R**) of participating solutes $[Ca^{2+}]_i$, $[Ca\text{-}Fluo]_i$, $[Fluo]_i$, $[Ca]_{SR}$, $[Ca\text{-}CSQ]_{SR}$, and $[Caff]_i$ (vector $\mathbf{u} = [u_1, \ldots u_6]$, respectively):

$$\frac{\partial \vec{\mathbf{u}}}{\partial t} = \frac{\partial}{\partial x}\left(\vec{\mathbf{D}} \cdot \frac{\partial \vec{\mathbf{u}}}{\partial x}\right) + \overrightarrow{\mathbf{R}(\mathbf{u})}. \quad (A2)$$

The model output for Ca^{2+}-bound Fluo-3 was used to best-fit experimental data (F/F_0). Ca^{2+} buffering in the myoplasm consisted of a lumped fast Ca^{2+} buffer, characterized empirically (29), and Fluo-3 (for details of Fluo-3 buffering see Fig. S1 in Data S1). Ca^{2+}-buffering in SR was attributed to calsequestrin (3). All participating solutes diffuse with their respective coefficients except calsequestrin, which is treated as immobile. In agreement with previous work (7,39–41), effective cytosolic Ca^{2+}-mobility in the presence of Fluo-3 was 16 $\mu m^2/s$ at resting $[Ca^{2+}]_i$. The unknown parameter elucidated in this study is D_{CaSR}. In the SR, free Ca^{2+} mobility is reduced by i) tortuosity (mobility reduced to D_{CaSR}^{tort}), and ii) buffering (mobility further reduced to D_{CaSR}) (32,42):

$$D_{CaSR} = D_{CaSR}^{tort} \times \left(1 + \frac{C_{csq} \times K_{csq}}{\left(K_{csq} + \left[Ca^{2+}\right]_{SR}\right)^2}\right)^{-1}.$$

Best-fitting experimental data yielded estimates for D_{CaSR}^{tort} and hence D_{CaSR} (Fig. 6 *B*). The latter was time-averaged over the period between partial and whole-cell caffeine exposure (Fig. 4).

Ca^{2+} can exit the SR passively through a leak pathway or a caffeine-activated RyR pathway (treated separately in the model). The position of the caffeine microstream is modeled using a discrete (0 or 1) function $S(x,t)$. SR leak was modeled as a first-order equation to account for local variations in SR leak during local SR depletion. The rate-constant of SR leak (k_{leak}) was derived empirically from experiments (Fig. 3 *Ci*). The model did not incorporate Ca^{2+}-flux through LCC or NCX as these were blocked in 0Na0Ca solutions. Ca^{2+} in the myoplasm can be sequestered into the SR by CPA-sensitive SERCA (3):

$$\mathbf{R} = \begin{bmatrix} \dfrac{(k_{leak} + u_6) \times (u_4 - u_1) - J_{SERCA} - J_{PMCA} + J_{bal} + k_{off}^{fluo} \times u_2 - k_{on}^{fluo} \times u_1 \times u_3}{1 + K_{buf} \times C_{buf} \times (K_{buf} + u_1)^{-2}} \\ k_{on}^{fluo} \times u_1 \times u_3 - k_{off}^{fluo} \times u_2 \\ k_{off}^{fluo} \times u_2 - k_{on}^{fluo} \times u_1 \times u_3 \\ (v_{myo}/v_{SR}) \times ((k_{leak} + u_6) \times (u_1 - u_4) + J_{SERCA}) - k_{on}^{csq} \times u_4 \times (C_{CSQ} - u_5) + k_{off}^{csq} \times u_5 \\ k_{on}^{csq} \times u_4 \times (C_{CSQ} - u_5) - k_{off}^{csq} \times u_5 \\ P_{caff} \times k_{rel} \times (S(x,t) - u_6) \end{bmatrix}.$$

$$J_{SERCA} = \frac{V_S^{max} \times \left(\left(\dfrac{[Ca^{2+}]_i}{K_S^f}\right)^{n_S} - \left(\dfrac{[Ca^{2+}]_{SR}}{K_S^r}\right)^{n_S}\right)}{1 + \left(\dfrac{[Ca^{2+}]_i}{K_S^f}\right)^{n_S} + \left(\dfrac{[Ca^{2+}]_{SR}}{K_S^r}\right)^{n_S}}.$$

In the presence of CPA, J_{SERCA} is set to zero. The model included a sarcolemmal PMCA pump and a net flux pathway (J_{bal}) to keep diastolic $[Ca^{2+}]$ at the desired level. To simulate Fig. 1 *B*, J_{bal} was set to 3.9 μM/s. The kinetics of the PMCA pump (based on previous work (43)) were scaled to fit the time course of $[Ca^{2+}]$ recovery in 0 Na0Ca solution with caffeine + CPA,

$$J_{PMCA} = \frac{V_P^{max} \times [Ca^{2+}]_i}{([Ca^{2+}]_i + K_P)}.$$

The reaction term in Eq. A2 is therefore (see Table 1 for parameter values),

Modeling a local SR Ca^{2+}-release event

The model includes SERCA and SR leak (but no PMCA activity), which are balanced to maintain $[Ca^{2+}]_i = 100$ nM. To simulate a localized microscopic SR release event lasting 250 ms, RyR permeability at a central 2 μm region of the SR was set to 1.35 μM/s (at this permeability, the SR depletes locally by 50% after 250 ms when $D_{CaSR} = 0$). The simulations were run for a range of D_{CaSR} (Fig. 7).

APPENDIX 2: LOCAL HETEROGENEITY OF D_{CaSR}: MODELING LUMINAL Ca^{2+} DIFFUSION IN SR NANOARCHITECTURE

Constructing nSR/jSR geometry

To approximate solute diffusion within the SR nanostructure of a sarcomere, we used the finite element method (Fig. 8 *Ai*) to solve Eq. A1 (for simplicity, SR leak was ignored). The geometry for a jSR cisterna and its connecting nSR tubes was derived from recent electron micrograph data (2). The jSR cisterna is modeled as a cylinder (2) of height 30 nm and diameter 592 nm and is connected, on average, to 4.3 nSR tubes. For the modeling here, we simplified this to a coupling ratio of 4 and represented the combination of jSR and nSR interaction as a sarcomeric ''unit'' (Fig. 8 *Ai*). Multiple units can be combined in 2-D to form a cellular SR network, as shown in Fig. 8 *Bi*. The SR geometry is thin along the *z* axis, so variation in the third dimension can be assumed to be negligible; therefore this 2-D model can approximate the three-dimensional solution. The jSR cisternae of individual units coincide with the Z-lines (2), whereas the nSR spans the distance in between. Although resting sarcomeres are 1.9 μm long (8), the nSR tubes may meander across the sarcomere and consequently be much longer and, thus, contribute to SR tortuosity.

The geometry of nSR tubes is not known in detail, but it must be compatible with the tortuosity imposed by the whole SR on unbuffered solute diffusion. Recent work has suggested that the environment of the ER in Chinese hamster ovary cells reduce mobility of green fluorescent protein, an unbuffered solute, by 2.6- to 6.2-fold, relative to cytosol (44). In cardiac myocytes, mobility of Fluo-5N in the SR (9) is 8 μm^2/s. The mobility of a related fluorophore, Fluo-3, in the cytoplasm has been estimated to be between 25 μm^2/s (allowing binding to muscle proteins) and 90 μm^2/s (without binding to muscle proteins) (40,45). SR Fluo-5N mobility is therefore between 3.1- and 11.3-fold lower than Fluo-3 mobility in cytoplasm. Based on green fluorescent protein and Fluo-5N mobility data, SR tortuosity is predicted to reduce mobility, on average, by a factor of 5.8 relative to cytoplasm, i.e., 11.6 relative to water (7).

Assuming that the nSR/jSR volume ratio is 1.1 (2), mean nSR half-length (ℓ, Fig. 8 *Ai*) and mean nSR tube radius (r) obey $\ell \times r^2 \approx 6.72 \times 10^{-4}$ nm^3. A 120-μm-long myocyte will contain 63 sarcomeres along its length and 10 sarcomeres across its width. A fully stretched nSR would be $126 \times \ell$ long in total. To determine nSR geometry, the geometrical model was run for a range of values of ℓ (hence r) until the geometry conformed to an 11.6-fold reduction in ''effective'' diffusion coefficient. Effective diffusion mobility was estimated by a simpler diffusive model, solved over a 1-D compartment as long as a myocyte, starting from a nonuniform initial concentration condition. Concentration was fixed at zero at one end of the SR along 25% of its length, whereas the remainder of the SR featured a reflection boundary condition and initial solute concentration of unity. Best-fit values for ℓ and r were 1.6 μm and 20 nm, respectively (Fig. 8 Ai). This would predict a 3.8 μm distance between cisternae centers, i.e., twice the intersarcomeric spacing. Thus, on the above model, nSR tubes would be predicted to meander and coil between adjacent cisternae, causing the measured level of SR tortuosity.

Modeling the kinetics of cisternal Ca^{2+} refilling

In rabbit myocytes, jSR refilling is proposed to occur with an average time constant of 29 ms, as derived from the time course of a Ca^{2+}-blink recovery (2). Recovery is too slow to be explained by rapid Ca^{2+} unbinding from calsequestrin (30) (i.e., buffer reequilibration); thus it is plausible to suggest that the time course of jSR Ca^{2+}-recovery is due to a diffusive process (2,14).

The geometry of a unit of SR (Fig. 8 *Ai*) can be used to approximate the kinetics of cisternal Ca^{2+} refilling. The half-length (ℓ) for nSR was set to 1.6 μm to simulate tortuosity (as described above). The SR unit was coupled to an infinite source of Ca^{2+}, implemented by introducing a constant concentration boundary condition at the distal ends of the nSR tubes (it is assumed that, for an isolated cisternal refilling event, the kinetics of SERCA are not rate limiting). To simulate jSR refilling, cisternal [Ca^{2+}] is rapidly halved and the recovery of jSR [Ca^{2+}] is modeled for a range of Ca^{2+}-diffusion coefficients at the jSR (D_{CajSR}) and nSR (D_{CanSR}). During Ca^{2+}-blinks, no change in nSR [Ca^{2+}] has been detected (2), implying a high local D_{CanSR} in the nSR. Our model can simulate the measured jSR refilling rate when D_{CajSR} is 1.8 $\mu m^2/s$ (see Fig. 8 *Aii*) and D_{CanSR} is equal to free Ca^{2+} mobility (1000 $\mu m^2/s$). Note that, during jSR refilling, the simulation predicts only a small (<3%) transient decrease of $[Ca^{2+}]_{SR}$ in the nSR elements. Further modeling (not shown) has revealed that similar refilling kinetics can be achieved for $D_{CanSR} > 300$ $\mu m^2/s$ without significant (<10%) nSR depletion.

Relationship between global Ca^{2+} mobility (D_{CaSR}) and jSR Ca^{2+} mobility (D_{CajSR})

To investigate the relationship between D_{CajSR} and global D_{CaSR}, we adopted the geometry (Fig. 8 *Bi*) based on a 63 × 10 array of nSR/jSR units (Fig. 8 *Ai*), i.e., proposing that the nSR meanders between Z-lines such that 3.2 μm of nSR spans a distance of 1.3 μm (sarcomere length, less jSR diameter). For this model, the nSR is assumed to be homogeneous, within which Ca^{2+} diffuses freely ($D_{Ca} = 1000$ $\mu m^2/s$ (7,28)). To drive diffusion, $[Ca^{2+}]_{SR}$ in one end of the SR (along 25% of the SR length) was set to 0.25 mM, simulating a localized exposure to caffeine (as illustrated in Fig. 8 *Bi*), and a zero-concentration boundary condition was imposed therein. The remainder of the SR featured a reflection boundary condition and initial concentration of 0.5 mM. The output of the model was then fitted with a simple diffusion equation, solved in a 120-μm-long homogeneous 1-D compartment with no geometrical restrictions, to derive ''effective'' mobility, i.e., the value for global D_{CaSR}. The predicted relationship between global D_{CaSR} and D_{CajSR} is plotted in Fig. 8 *Bii*.

In an extension to our SR model, we incorporated heterogeneity of Ca^{2+}-mobility in nSR (Fig. 8 *Biii*) with fast (1000 $\mu m^2/s$) diffusion in *snSR* and restricted diffusion (<1000 $\mu m^2/s$) in the intersarcomeric nSR (*inSR*). The value of the latter cannot be determined without a detailed geometrical description. However, overall nSR Ca^{2+}-mobility, averaged over its length, must be 110 $\mu m^2/s$ to be consistent with the estimated D_{CajSR} and measured global D_{CaSR}. The effect of restricted *inSR* Ca^{2+}-diffusion on overall Ca^{2+}-mobility is maximized when nSR half-length ℓ is minimal, i.e., 0.65 μm (as short as the Z-line to Z-line spacing permits minus cisterna diameter). By modeling this scenario, we found that the percentage of total nSR length occupied by *inSR* would equal *inSR* Ca^{2+}-mobility (expressed in $\mu m^2/s$) multiplied by 0.85%. If, for example, Ca^{2+}-mobility in *inSR* was comparable to D_{CajSR}, the *inSR* would occupy 1.5% of the nSR length.

SUPPLEMENTARY MATERIAL

To view all of the supplemental files associated with this article, visit www.biophysj.org.

We thank Philip Cobden for excellent technical assistance.

We thank the British Heart Foundation (Programme Grant to R.D.V.-J.), National Institutes of Health (MERIT award 5R37HL042873 to K.W.S.), and the Nora Eccles Treadwell Foundation (K.W.S.).

REFERENCES

1. Page, E. 1978. Quantitative ultrastructural analysis in cardiac membrane physiology. *Am. J. Physiol.* 235:C147–C158.
2. Brochet, D. X., D. Yang, A. Di Maio, W. J. Lederer, C. Franzini-Armstrong, and H. Cheng. 2005. Ca^{2+} blinks: rapid nanoscopic store calcium signaling. *Proc. Natl. Acad. Sci. USA.* 102:3099–3104.
3. Shannon, T. R., K. S. Ginsburg, and D. M. Bers. 2000. Reverse mode of the sarcoplasmic reticulum calcium pump and load-dependent cytosolic calcium decline in voltage-clamped cardiac ventricular myocytes. *Biophys. J.* 78:322–333.
4. Bers, D. M. 2002. Sarcoplasmic reticulum Ca^{2+} release in intact ventricular myocytes. *Front. Biosci.* 7:1697–1711.
5. Stern, M. D. 1992. Theory of excitation-contraction coupling in cardiac muscle. *Biophys. J.* 63:497–517.
6. Cheng, H., W. J. Lederer, and M. B. Cannell. 1993. Calcium sparks: elementary events underlying excitation-contraction coupling in heart muscle. *Science.* 262:740–744.
7. Kushmerick, M. J., and R. J. Podolsky. 1969. Ionic mobility in muscle cells. *Science.* 166:1297–1298.
8. Shannon, T. R., T. Guo, and D. M. Bers. 2003. Ca^{2+} scraps: local depletions of free [Ca^{2+}] in cardiac sarcoplasmic reticulum during contractions leave substantial Ca^{2+} reserve. *Circ. Res.* 93:40–45.
9. Wu, X., and D. M. Bers. 2006. Sarcoplasmic reticulum and nuclear envelope are one highly interconnected Ca^{2+} store throughout cardiac myocyte. *Circ. Res.* 99:283–291.
10. Meissner, G. 1975. Isolation and characterization of two types of sarcoplasmic reticulum vesicles. *Biochim. Biophys. Acta.* 389:51–68.
11. Scriven, D. R., P. Dan, and E. D. Moore. 2000. Distribution of proteins implicated in excitation-contraction coupling in rat ventricular myocytes. *Biophys. J.* 79:2682–2691.
12. Keller, M., J. P. Kao, M. Egger, and E. Niggli. 2007. Calcium waves driven by ''sensitization'' wave-fronts. *Cardiovasc. Res.* 74:39–45.
13. Kubalova, Z., D. Terentyev, S. Viatchenko-Karpinski, Y. Nishijima, I. Gyorke, R. Terentyeva, D. N. da Cunha, A. Sridhar, D. S. Feldman, R. L. Hamlin, C. A. Carnes, and S. Gyorke. 2005. Abnormal intrastore calcium signaling in chronic heart failure. *Proc. Natl. Acad. Sci. USA.* 102:14104–14109.
14. Niggli, E., and N. Shirokova. 2007. A guide to sparkology: the taxonomy of elementary cellular Ca^{2+} signaling events. *Cell Calcium.* 42:379–387.
15. Venetucci, L., A. W. Trafford, and D. A. Eisner. 2003. Illuminating sarcoplasmic reticulum calcium. *Circ. Res.* 93:4–5.
16. Spitzer, K. W., P. R. Ershler, R. L. Skolnick, and R. D. Vaughan-Jones. 2000. Generation of intracellular pH gradients in single cardiac myocytes with a microperfusion system. *Am. J. Physiol. Heart Circ. Physiol.* 278:H1371–H1382.
17. Swietach, P., and R. D. Vaughan-Jones. 2005. Relationship between intracellular pH and proton mobility in rat and guinea-pig ventricular myocytes. *J. Physiol.* 566:793–806.
18. Bassani, R. A., and D. M. Bers. 1995. Rate of diastolic Ca release from the sarcoplasmic reticulum of intact rabbit and rat ventricular myocytes. *Biophys. J.* 68:2015–2022.
19. Bassani, R. A., J. W. Bassani, and D. M. Bers. 1992. Mitochondrial and sarcolemmal Ca^{2+} transport reduce $[Ca^{2+}]_i$ during caffeine contractures in rabbit cardiac myocytes. *J. Physiol.* 453:591–608.
20. Rousseau, E., and G. Meissner. 1989. Single cardiac sarcoplasmic reticulum Ca^{2+}-release channel: activation by caffeine. *Am. J. Physiol.* 256:H328–H333.
21. Berlin, J. R., J. W. Bassani, and D. M. Bers. 1994. Intrinsic cytosolic calcium buffering properties of single rat cardiac myocytes. *Biophys. J.* 67:1775–1787.
22. Shannon, T. R., K. S. Ginsburg, and D. M. Bers. 2002. Quantitative assessment of the SR Ca^{2+} leak-load relationship. *Circ. Res.* 91:594–600.
23. Nieman, C. J., and D. A. Eisner. 1985. Effects of caffeine, tetracaine, and ryanodine on calcium-dependent oscillations in sheep cardiac Purkinje fibers. *J. Gen. Physiol.* 86:877–889.
24. Spitzer, K. W., and J. H. Bridge. 1989. A simple device for rapidly exchanging solution surrounding a single cardiac cell. *Am. J. Physiol.* 256:C441–C447.

25. Swietach, P., C. H. Leem, K. W. Spitzer, and R. D. Vaughan-Jones. 2005. Experimental generation and computational modeling of intracellular pH gradients in cardiac myocytes. *Biophys. J.* 88:3018–3037.

26. O'Neill, S. C., P. Donoso, and D. A. Eisner. 1990. The role of $[Ca^{2+}]_i$ and $[Ca^{2+}]$ sensitization in the caffeine contracture of rat myocytes: measurement of $[Ca^{2+}]_i$ and $[caffeine]_i$. *J. Physiol.* 425:55–70.

27. O'Neill, S. C., and D. A. Eisner. 1990. A mechanism for the effects of caffeine on Ca^{2+} release during diastole and systole in isolated rat ventricular myocytes. *J. Physiol.* 430:519–536.

28. Vanysek, P. 1999. Ionic conductivity and diffusion at infinite dilution. *In* CRC Handbook of Chemistry and Physics, Thermochemistry, Electrochemistry and Kinetics. D. R. Lide, editor. CRC, London. 93–95.

29. Trafford, A. W., M. E. Diaz, and D. A. Eisner. 1999. A novel, rapid and reversible method to measure Ca^{2+} buffering and time-course of total sarcoplasmic reticulum Ca^{2+} content in cardiac ventricular myocytes. *Pflugers Arch.* 437:501–503.

30. Beltran, M., G. Barrientos, and C. Hidalgo. 2006. Fast kinetics of calcium dissociation from calsequestrin. *Biol. Res.* 39:493–503.

31. Shannon, T. R., and D. M. Bers. 1997. Assessment of intra-SR free $[Ca^{2+}]$ and buffering in rat heart. *Biophys. J.* 73:1524–1531.

32. Gabso, M., E. Neher, and M. E. Spira. 1997. Low mobility of the Ca^{2+} buffers in axons of cultured Aplysia neurons. *Neuron.* 18:473–481.

33. Stern, M. D., and H. Cheng. 2004. Putting out the fire: what terminates calcium-induced calcium release in cardiac muscle? *Cell Calcium.* 35: 591–601.

34. Terentyev, D., S. Viatchenko-Karpinski, H. H. Valdivia, A. L. Escobar, and S. Gyorke. 2002. Luminal Ca^{2+} controls termination and refractory behavior of Ca^{2+}-induced Ca^{2+} release in cardiac myocytes. *Circ. Res.* 91:414–420.

35. Knollmann, B. C., N. Chopra, T. Hlaing, B. Akin, T. Yang, K. Ettensohn, B. E. Knollmann, K. D. Horton, N. J. Weissman, I. Holinstat, W. Zhang, D. M. Roden, L. R. Jones, C. Franzini-Armstrong, and K. Pfeifer. 2006. Casq2 deletion causes sarcoplasmic reticulum volume increase, premature Ca^{2+} release, and catecholaminergic polymorphic ventricular tachycardia. *J. Clin. Invest.* 116:2510–2520.

36. Wang, W., L. Cleemann, L. R. Jones, and M. Morad. 2000. Modulation of focal and global Ca^{2+} release in calsequestrin-overexpressing mouse cardiomyocytes. *J. Physiol.* 524:399–414.

37. Diaz, M. E., D. A. Eisner, and S. C. O'Neill. 2002. Depressed ryanodine receptor activity increases variability and duration of the systolic Ca^{2+} transient in rat ventricular myocytes. *Circ. Res.* 91: 585–593.

38. Sobie, E. A., L. S. Song, and W. J. Lederer. 2006. Restitution of Ca^{2+} release and vulnerability to arrhythmias. *J. Cardiovasc. Electrophysiol.* 17(Suppl 1):S64–S70.

39. Baylor, S. M., and S. Hollingworth. 1998. Model of sarcomeric Ca^{2+} movements, including ATP Ca^{2+} binding and diffusion, during activation of frog skeletal muscle. *J. Gen. Physiol.* 112:297–316.

40. Cordeiro, J. M., K. W. Spitzer, W. R. Giles, P. E. Ershler, M. B. Cannell, and J. H. Bridge. 2001. Location of the initiation site of calcium transients and sparks in rabbit heart Purkinje cells. *J. Physiol.* 531:301–314.

41. Allbritton, N. L., T. Meyer, and L. Stryer. 1992. Range of messenger action of calcium ion and inositol 1,4,5-trisphosphate. *Science.* 258: 1812–1815.

42. Wagner, J., and J. Keizer. 1994. Effects of rapid buffers on Ca^{2+} diffusion and Ca^{2+} oscillations. *Biophys. J.* 67:447–456.

43. Shannon, T. R., F. Wang, J. Puglisi, C. Weber, and D. M. Bers. 2004. A mathematical treatment of integrated Ca dynamics within the ventricular myocyte. *Biophys. J.* 87:3351–3371.

44. Dayel, M. J., E. F. Hom, and A. S. Verkman. 1999. Diffusion of green fluorescent protein in the aqueous-phase lumen of endoplasmic reticulum. *Biophys. J.* 76:2843–2851.

45. Harkins, A. B., N. Kurebayashi, and S. M. Baylor. 1993. Resting myoplasmic free calcium in frog skeletal muscle fibers estimated with fluo-3. *Biophys. J.* 65:865–881.

46. Hinch, R., J. L. Greenstein, A. J. Tanskanen, L. Xu, and R. L. Winslow. 2004. A simplified local control model of calcium-induced calcium release in cardiac ventricular myocytes. *Biophys. J.* 87:3723–3736.

47. Satoh, H., L. M. Delbridge, L. A. Blatter, and D. M. Bers. 1996. Surface:volume relationship in cardiac myocytes studied with confocal microscopy and membrane capacitance measurements: species-dependence and developmental effects. *Biophys. J.* 70:1494–1504.

48. Page, E., L. P. McCallister, and B. Power. 1971. Sterological measurements of cardiac ultrastructures implicated in excitation-contraction coupling. *Proc. Natl. Acad. Sci. USA.* 68:1465–1466.

49. Soeller, C., and M. B. Cannell. 1999. Examination of the transverse tubular system in living cardiac rat myocytes by 2-photon microscopy and digital image-processing techniques. *Circ. Res.* 84:266–275.

50. Snyder, S. M., B. M. Palmer, and R. L. Moore. 2000. A mathematical model of cardiocyte Ca^{2+} dynamics with a novel representation of sarcoplasmic reticular Ca^{2+} control. *Biophys. J.* 79:94–115.